GNSS Positioning Safety
Probability of Positioning Failure and its Components

Ciuban, Sebastian; Teunissen, Peter J.G.; Tiberius, Christian C.J.M.

DOI
10.33012/2024.19794

Publication date
2024

Document Version
Final published version

Published in
Proceedings of the 37th International Technical Meeting of the Satellite Division of The Institute of Navigation (ION GNSS+ 2024)

Citation (APA)
Ciuban, S., Teunissen, P. J. G., & Tiberius, C. C. J. M. (2024). GNSS Positioning Safety: Probability of Positioning Failure and its Components. In *Proceedings of the 37th International Technical Meeting of the Satellite Division of The Institute of Navigation (ION GNSS+ 2024)* (pp. 2228 - 2249). Institute of Navigation. https://doi.org/10.33012/2024.19794

GNSS Positioning Safety: Probability of Positioning Failure and its Components

Sebastian Ciuban, Peter J.G. Teunissen, Christian C.J.M. Tiberius, *Delft University of Technology*

BIOGRAPHY

Sebastian Ciuban is a Ph.D. candidate at Delft University of Technology, The Netherlands, focusing on GNSS safe-positioning for automotive applications. He received his M.Sc. in Aerospace Systems: Navigation and Telecommunications from École Nationale de l'Aviation Civile, Toulouse, France, in 2017. Afterwards, he joined ESA-ESTEC as a Young Graduate Trainee. From 2019 to 2021, he worked as a GNSS Engineer at CGI Nederland. His research interests include the interplay between parameter estimation and statistical hypothesis testing, numerical integration methods, and positioning-safety analyses.

Peter J.G. Teunissen is Professor of Geodesy and Satellite Navigation at Delft University of Technology, The Netherlands, and a member of the Royal Netherlands Academy of Arts and Sciences. Previously, he was Head of the Delft Earth Observation Institute, Science Director of the Australian Centre for Spatial Information, and Federation Fellow of the Australian Research Council. His current research focuses on developing theory, models, and algorithms for high-accuracy satellite navigation and remote sensing applications.

Christian C.J.M. Tiberius received the Ph.D. degree on the subject of recursive data processing for kinematic GPS surveying from the Delft University of Technology, Delft, The Netherlands, in 1998. He is currently an Associate Professor at the Geoscience and Remote Sensing (GRS) Department, Delft University of Technology. His research interests include navigation, with GNSS and terrestrial radio positioning, primarily for automotive applications.

ABSTRACT

GNSS-based positioning plays an important role in safety-critical applications (e.g., automotive, aviation, shipping, rail) where positioning safety is paramount. Safety analyses typically include a probability-based formulation, such as calculating the probability that the position estimator falls outside a safety region (probability of positioning failure). Once this probability is being computed, it can be compared to an application specific requirement to decide whether or not this requirement is met. In this context, we carry out a component-wise analysis of the probability of positioning failure for the Detection, Identification, and Adaptation (DIA) estimator. The probability of positioning failure is formulated based on the DIA estimator's probability density function (PDF) which accounts for the dependence between parameter estimation and statistical hypothesis testing. The probability of positioning failure can be further expressed in terms of its conditional components via the law of total probability which enables the assessment of the Most Impactful Components (MICs). Knowledge about the MICs can be useful to determine the main contributors to the probability of positioning failure. Using a dual GNSS (GPS and Galileo) positioning model for an automated vehicle, we compute the MICs based on the conditional PDFs components of the DIA estimator. Furthermore, we determine the worst-case scenario by computing the maximum total probability of positioning failure over a range of magnitudes for the outliers in the observables and over different orientations of the vehicle. These types of analyses can be useful during the design stage of DIA estimators to verify whether the safety requirements for positioning are met. Lastly, we summarize our contributions and provide an outlook on future work.

I. INTRODUCTION

Global Navigation Satellite Systems (GNSS) are used in several safety-critical applications, including automotive, aviation, shipping, and rail (Teunissen and Montenbruck, 2017; Morton et al., 2020). For a position estimator $\underline{\bar{x}} \in \mathbb{R}^n$ and an application-dependent safety-region $\mathcal{B} \subset \mathbb{R}^n$ centered at the true position, the event of *positioning failure* can be expressed as (based on the definition provided on page 15 in (RTCA-Special Committee 159, 2020))

$$\mathcal{F} = \{\underline{\bar{x}} \notin \mathcal{B}\} = \{\underline{\bar{x}} \in \mathcal{B}^c\}, \tag{1}$$

where $\mathcal{B}^c = \mathbb{R}^n \backslash \mathcal{B}$ is the failure-region and the contour of $\mathcal{B} \subset \mathbb{R}^n$ defines the Alert Limit (e.g., ellipse in $\mathbb{R}^{n=2}$). Having access to the probability density function (PDF) of the position estimator $\underline{\bar{x}}$, denoted $f_{\underline{\bar{x}}}(x)$, the probability of positioning failure is

$$\mathbb{P}_{\mathcal{F}} = \mathsf{P}(\underline{\bar{x}} \in \mathcal{B}^c) = \int_{\mathcal{B}^c} f_{\underline{\bar{x}}}(x)\, dx. \tag{2}$$

On the basis of (2), positioning safety-analyses can be conducted, and the results obtained can be used to verify compliance with respect to (w.r.t.) application-specific requirements or guidelines (e.g., for automotive (Reid et al., 2019), for aviation (RTCA-Special Committee 159, 2020)). The computation, analysis, and validation of the results based on (2) align with the scenario-based safety assessment framework used for automated and autonomous vehicles (Riedmaier et al., 2020; U.N.E.C.E., 2023; de Gelder et al., 2024). Following this framework, we conduct positioning safety-analyses at the design stage, when choices are to be made regarding (i) measurement models, (ii) parameter estimation algorithms, (iii) statistical hypothesis testing procedures for model misspecifications (e.g., outliers or faults in measurements), and (iv) positioning scenarios for vehicles, among other considerations. The computation and analysis of (2) rely on numerical simulations due to the complexity of the multiple integral(s) and the impracticality of collecting the necessary measurements or data (e.g., for automotive applications it would require millions or even billions of kilometers of driving (Kalra and Paddock, 2016)). Once compliance with the application-specific requirements is demonstrated on the basis of the probability of positioning failure in the scenarios of interest, the resulting parameter estimation and statistical hypothesis testing procedure can be implemented for real-time positioning.

As the position estimator $\bar{\underline{x}}$ is often the outcome of parameter estimation and a statistical hypothesis testing procedure for model misspecifications (e.g., a Detection, Identification, and Adaptation-DIA procedure (Baarda, 1968; Gillissen and Elema, 1996; Teunissen, 2017) or a Fault Detection and Exclusion-FDE procedure (Hwang and Brown, 2006; Blanch et al., 2015; Yang et al., 2013)), it is important to account for the *dependence* between these two statistical inference concepts in the PDF $f_{\bar{\underline{x}}}(x)$. By neglecting this dependence in $f_{\bar{\underline{x}}}(x)$, one may obtain unrepresentative (e.g., over-optimistic) results when assessing the quality of $\bar{\underline{x}}$ (Zaminpardaz and Teunissen, 2022). The importance of accounting for this dependence has been recognized in various fields, including mathematical statistics, econometrics, and signal processing (Bancroft, 1944; Danilov and Magnus, 2004; Routtenberg and Tong, 2016).

A theoretical framework addressing the dependence between parameter estimation and statistical hypothesis testing has been introduced in (Teunissen, 2018). In this framework, the expressions for $\bar{\underline{x}}$ (referred to as the DIA-estimator) and $f_{\bar{\underline{x}}}(x)$ are derived. Considering a multiple hypothesis testing procedure, where a null hypothesis $\mathcal{H}_0$ is tested against multiple alternative hypotheses $\mathcal{H}_i$ for $i \in \{1, ..., k\}$, the PDF of the DIA-estimator can be decomposed via the rule of total probability

$$f_{\bar{\underline{x}}}(x) = \mathsf{P}(\mathcal{H}_0) f_{\bar{\underline{x}}}(x|\mathcal{H}_0) + \sum_{i=1}^{k} \mathsf{P}(\mathcal{H}_i) f_{\bar{\underline{x}}}(x|\mathcal{H}_i), \tag{3}$$

where $\mathsf{P}(\mathcal{H}_0)$ and $\mathsf{P}(\mathcal{H}_i)$ are the a-priori probability of occurrence of the hypotheses. A further decomposition of $f_{\bar{\underline{x}}}(x|\mathcal{H}_0)$ and $f_{\bar{\underline{x}}}(x|\mathcal{H}_i)$ gives

$$f_{\bar{\underline{x}}}(x|\mathcal{H}) = \begin{cases} \mathsf{P}_{\mathrm{CA}} f_{\bar{\underline{x}}|\mathrm{CA}}(x|\mathrm{CA}) + \sum_{j=1}^{k} \mathsf{P}_{\mathrm{FA}_j} f_{\bar{\underline{x}}|\mathrm{FA}_j}(x|\mathrm{FA}_j) & \text{if } \mathcal{H} = \mathcal{H}_0 \\ \mathsf{P}_{\mathrm{MD}_i} f_{\bar{\underline{x}}|\mathrm{MD}_i}(x|\mathrm{MD}_i) + \mathsf{P}_{\mathrm{CI}_i} f_{\bar{\underline{x}}|\mathrm{CI}_i}(x|\mathrm{CI}_i) + \sum_{j\neq 0,i}^{k} \mathsf{P}_{\mathrm{WI}_j} f_{\bar{\underline{x}}|\mathrm{WI}_j}(x|\mathrm{WI}_j) & \text{if } \mathcal{H} = \mathcal{H}_i \end{cases}, \tag{4}$$

where (a) under $\mathcal{H}_0$: $f_{\bar{\underline{x}}|\mathrm{CA}}(x|\mathrm{CA})$ and $f_{\bar{\underline{x}}|\mathrm{FA}_i}(x|\mathrm{FA}_i)$ are the conditional PDFs on the testing decisions of Correct Acceptance (CA) when $\mathcal{H}_0$ is accepted and of False Alarm (FA) when $\mathcal{H}_0$ is rejected and $\mathcal{H}_i$ is accepted; P_{CA} and $\mathsf{P}_{\mathrm{FA}_i}$ are the probabilities of the events of CA and of FA per $\mathcal{H}_i$, (b) under $\mathcal{H}_i$: $f_{\bar{\underline{x}}|\mathrm{MD}_i}(x|\mathrm{MD}_i)$, $f_{\bar{\underline{x}}|\mathrm{CI}_i}(x|\mathrm{CI}_i)$, and $f_{\bar{\underline{x}}|\mathrm{WI}_j}(x|\mathrm{WI}_j)$ are the conditional PDFs on the testing decisions of Missed Detection (MD) when $\mathcal{H}_0$ is accepted, Correct Identification (CI) when $\mathcal{H}_0$ is rejected and $\mathcal{H}_i$ is accepted, and Wrong Identification (WI) when $\mathcal{H}_0$ is rejected and $\mathcal{H}_j$ is accepted for $j \notin \{0, i\}$; $\mathsf{P}_{\mathrm{MD}_i}$, $\mathsf{P}_{\mathrm{CI}_i}$, and $\mathsf{P}_{\mathrm{WI}_j}$ are the probabilities of the corresponding events. Based on (3) and (4) the probability of positioning failure can be expressed as

$$\mathbb{P}_{\mathcal{F}} = \mathsf{P}(\mathcal{H}_0)\left(\int_{\mathcal{B}^c} f_{\bar{\underline{x}}}(x|\mathcal{H}_0)\,dx\right) + \sum_{i=1}^{k} \mathsf{P}(\mathcal{H}_i)\left(\int_{\mathcal{B}^c} f_{\bar{\underline{x}}}(x|\mathcal{H}_i)\,dx\right) = \mathsf{P}(\mathcal{H}_0)\mathbb{P}_{\mathcal{F}}|\mathcal{H}_0 + \sum_{i=1}^{k} \mathsf{P}(\mathcal{H}_i)\mathbb{P}_{\mathcal{F}}|\mathcal{H}_i, \tag{5}$$

where,

$$\mathbb{P}_{\mathcal{F}}|\mathcal{H} = \begin{cases} \mathsf{P}_{\mathrm{CA}}\mathbb{P}_{\mathcal{F}}|\mathrm{CA} + \sum_{j=1}^{k} \mathsf{P}_{\mathrm{FA}_j}\mathbb{P}_{\mathcal{F}}|\mathrm{FA}_j & \text{if } \mathcal{H} = \mathcal{H}_0 \\ \mathsf{P}_{\mathrm{MD}_i}\mathbb{P}_{\mathcal{F}}|\mathrm{MD}_i + \mathsf{P}_{\mathrm{CI}_i}\mathbb{P}_{\mathcal{F}}|\mathrm{CI}_i + \sum_{j\neq 0,i}^{k} \mathsf{P}_{\mathrm{WI}_j}\mathbb{P}_{\mathcal{F}}|\mathrm{WI}_j & \text{if } \mathcal{H} = \mathcal{H}_i \end{cases}. \tag{6}$$

One can use (6) to determine which components (or terms) are the most or least influential to $\mathbb{P}_{\mathcal{F}}|\mathcal{H}$. Knowledge about the Most Influential Components (MICs) and/or Least Influential Components (LICs) of $\mathbb{P}_{\mathcal{F}}|\mathcal{H}$ can be valuable at the design stages of the algorithms for parameter estimation and statistical hypothesis testing (e.g., a DIA-estimator). Note that at this stage, the MICs and LICs are intrinsic to the designed DIA-estimator and do not depend on the 'weighting' given by the a priori probabilities. Having determined the values of $\mathbb{P}_{\mathcal{F}}|\mathcal{H}$, the total probability of failure $\mathbb{P}_{\mathcal{F}}$ can then be calculated using the a priori probabilities $\mathsf{P}(\mathcal{H})$ and used to verify compliance with application-specific requirements or guidelines. In this contribution, we quantify the MIC/LICs, $\mathbb{P}_{\mathcal{F}}|\mathcal{H}$, and $\mathbb{P}_{\mathcal{F}}$ in a GNSS-based (decimeter level) positioning scenario of an automated vehicle.

This article is organized as follows: In Section II we review the main principles of the DIA-estimator $\bar{\underline{\mathrm{x}}} \in \mathbb{R}^n$ and its PDF $f_{\bar{\underline{\mathrm{x}}}}(x)$. Section III presents the probability of positioning failure and its conditional components based on the PDF $f_{\bar{\underline{\mathrm{x}}}}(x)$. Section IV contains two examples in which we apply the principles outlined in this contribution. The first example is intended to illustrate the integration regions involved in computing the probability of positioning failure via a simple one-dimensional positioning problem. In the second example, we carry out a positioning safety analysis for an automated vehicle whose position vector is determined, at the decimetre level, based on GNSS (GPS and Galileo). In both examples, the MICs/LICs, $\mathbb{P}_{\mathcal{F}}|\mathcal{H}$, and $\mathbb{P}_{\mathcal{F}}$ are quantified. Also, the probability of positioning failure is computed for a worst-case scenario based on which conclusions can be drawn whether the results are compliant with positioning safety targets or requirements. In Section V we summarize our contribution and provide an outlook on future work.

Throughout the paper we make use of the following notation: an underscore denotes a random quantity (e.g., the random vector $\underline{\mathrm{x}} \in \mathbb{R}^n$), $f_{\underline{\mathrm{x}}}(x)$ is the PDF of $\underline{\mathrm{x}} \in \mathbb{R}^n$, $\mathsf{E}_{f_{\underline{\mathrm{x}}}}(\underline{\mathrm{x}}) = \int_{\mathbb{R}^n} x f_{\underline{\mathrm{x}}}(x)dx$ is the expectation of $\underline{\mathrm{x}} \in \mathbb{R}^n$, and $\mathrm{Q}_{\mathrm{xx}} \in \mathbb{R}^{n\times n}$ is the variance-covariance matrix of $\underline{\mathrm{x}} \in \mathbb{R}^n$. The joint PDF of two random vectors $\underline{\mathrm{x}} \in \mathbb{R}^n$ and $\underline{\mathrm{y}} \in \mathbb{R}^m$ is denoted $f_{\underline{\mathrm{x}},\underline{\mathrm{y}}}(x, y)$. The PDF of a random vector $\underline{\mathrm{x}}$ conditioned on an event $\mathcal{E}$ is written as $f_{\underline{\mathrm{x}}|\mathcal{E}}(x|\mathcal{E})$. The probability of an event $\mathcal{E}$ is denoted $\mathsf{P}_{\mathcal{E}} = \mathsf{P}(\mathcal{E})$. A projection matrix is expressed as $\mathbf{Q}_{\mathrm{A}}$ and it projects orthogonally (w.r.t. some metric) onto the range space of the matrix $\mathrm{A} \in \mathbb{R}^{m\times n}$ ($\mathcal{R}(\mathrm{A})$). For the weighted squared norm of a vector we use the notation $||.||^2_{\mathrm{Q}} = (.)^T\mathrm{Q}^{-1}(.)$. If the squared norm is w.r.t. the identity matrix then it is denoted $||.||^2$.

II. REVIEW OF DETECTION, IDENTIFICATION, AND ADAPTATION (DIA) ESTIMATOR

In this section we review the principles of the *Distributional theory for the DIA-method* as introduced in (Teunissen, 2018). Consider a random vector of observables $\underline{\mathrm{y}} \in \mathbb{R}^m$ which it is assumed to be normally distributed $\underline{\mathrm{y}} \sim \mathcal{N}(\mathrm{Ax}, \mathrm{Q}_{\mathrm{yy}})$, where: (i) $\mathrm{A} \in \mathbb{R}^{m\times n}$ is the design matrix with $\mathrm{rank}(\mathrm{A}) = n$, (ii) $\mathrm{x} \in \mathbb{R}^n$ is the vector of unknown parameters (e.g., receiver coordinate increments, receiver clock bias), and (iii) $\mathrm{Q}_{\mathrm{yy}} \in \mathbb{R}^{m\times m}$ is a symmetric positive definite variance-covariance matrix of $\underline{\mathrm{y}} \in \mathbb{R}^m$. It is common that in practice model misspecifications of the mean of $\underline{\mathrm{y}}$ (e.g., due to outliers) occur (Teunissen, 2017). On this basis, the following multiple statistical hypothesis testing problem is formulated,

$$\mathcal{H}_0 : \mathsf{E}_{f_{\underline{\mathrm{y}}}}(\underline{\mathrm{y}}) = \mathrm{Ax} \quad \text{vs.} \quad \mathcal{H}_i : \mathsf{E}_{f_{\underline{\mathrm{y}}}}(\underline{\mathrm{y}}) = \mathrm{Ax} + \mathrm{C}_i\mathrm{b}_i \quad \text{for } i \in \{1, ..., k\}, \tag{7}$$

where $\mathrm{C}_i \in \mathbb{R}^{m\times q_i}$ models the type of model misspecification, $\mathrm{rank}([\mathrm{A}, \mathrm{C}_i]) = n + q_i$, $\mathrm{b}_i \in \mathbb{R}^{q_i}$ is the model misspecification (e.g., outlier(s) in the observable(s)), and $1 \leq q_i \leq r$ for $i > 0$ (to allow for parameter estimation under $\mathcal{H}_i$) with $r = m - \mathrm{rank}(\mathrm{A})$ being the redundancy of $\mathcal{H}_0$. The expressions of the Best Linear Unbiased Estimators (BLUEs) of the unknown parameter vector $\mathrm{x} \in \mathbb{R}^n$ are

$$\underline{\hat{\mathrm{x}}}_0 = \mathrm{A}^+\,\underline{\mathrm{y}} \text{ (under } \mathcal{H}_0) \quad \text{and} \quad \underline{\hat{\mathrm{x}}}_i = \bar{\mathrm{A}}_i^+\,\underline{\mathrm{y}} \text{ (under } \mathcal{H}_i), \tag{8}$$

where $\mathrm{A}^+ = \mathrm{Q}_{\hat{\mathrm{x}}_0\hat{\mathrm{x}}_0}\mathrm{A}^T\mathrm{Q}_{\mathrm{yy}}^{-1}$ is the BLUE-inverse of A, $\mathrm{Q}_{\hat{\mathrm{x}}_0\hat{\mathrm{x}}_0} = (\mathrm{A}^T\mathrm{Q}_{\mathrm{yy}}^{-1}\mathrm{A})^{-1}$ is the variance-covariance matrix of $\underline{\hat{\mathrm{x}}}_0$, $\bar{\mathrm{A}}_i^+ = \mathrm{Q}_{\hat{\mathrm{x}}_i\hat{\mathrm{x}}_i}\bar{\mathrm{A}}_i^T\mathrm{Q}_{\mathrm{yy}}^{-1}$, $\mathrm{Q}_{\hat{\mathrm{x}}_i\hat{\mathrm{x}}_i} = (\bar{\mathrm{A}}_i^T\mathrm{Q}_{\mathrm{yy}}^{-1}\bar{\mathrm{A}}_i)^{-1}$ is the variance-covariance matrix of $\underline{\hat{\mathrm{x}}}_i$, $\bar{\mathrm{A}}_i = \mathbf{Q}_{\mathrm{C}_i}^{\perp}\mathrm{A}$, and $\mathbf{Q}_{\mathrm{C}_i}^{\perp} = \mathrm{I}_m - \mathrm{C}_i(\mathrm{C}_i^T\mathrm{Q}_{\mathrm{yy}}^{-1}\mathrm{C}_i)^{-1}\mathrm{C}_i^T\mathrm{Q}_{\mathrm{yy}}^{-1}$ is the orthogonal projector (w.r.t. the metric of $\mathrm{Q}_{\mathrm{yy}}^{-1}$) that projects onto $\mathcal{R}(\mathrm{C}_i)^{\perp}$ (the orthogonal complement of $\mathcal{R}(\mathrm{C}_i)$). A realized value of the estimator $\underline{\hat{\mathrm{x}}}_i$, for $i \in \{0, ..., k\}$, is called an estimate and its notation is $\hat{\mathrm{x}}_i$. To build test statistics for the decision problem in (7) one can use the *vector of misclosures* or *misclosure vector* (Teunissen, 2024b)

$$\underline{\mathrm{t}} = \mathrm{B}^T\underline{\mathrm{y}}, \quad \mathrm{Q}_{\mathrm{tt}} = \mathrm{B}^T\mathrm{Q}_{\mathrm{yy}}\mathrm{B}, \tag{9}$$

with $\mathrm{B} \in \mathbb{R}^{m\times r}$ of $\mathrm{rank}(\mathrm{B}) = r$ and $\mathrm{B}^T\mathrm{A} = 0_{r\times n}$. The vector of misclosures provides a measure of inconsistency between the model under $\mathcal{H}_0$ and the observations. Furthermore, the vector of misclosures can be used to link the BLUEs in (8) via the following invertible transformation

$$\begin{bmatrix} \underline{\hat{\mathrm{x}}}_i \\ \underline{\mathrm{t}} \end{bmatrix} = \begin{bmatrix} \mathrm{I}_n & -\mathrm{L}_i \\ 0_{r\times n} & \mathrm{I}_r \end{bmatrix} \begin{bmatrix} \underline{\hat{\mathrm{x}}}_0 \\ \underline{\mathrm{t}} \end{bmatrix}, \text{ with } \mathrm{L}_i = \begin{cases} 0_{n\times r} & , i = 0 \\ \mathrm{A}^+\mathrm{C}_i\mathrm{C}_{\mathrm{t}_i}^+ & , i > 0 \end{cases}, \tag{10}$$

and $\mathrm{C}_{\mathrm{t}_i}^+ = (\mathrm{C}_{\mathrm{t}_i}^T\mathrm{Q}_{\mathrm{tt}}^{-1}\mathrm{C}_{\mathrm{t}_i})^{-1}\mathrm{C}_{\mathrm{t}_i}^T\mathrm{Q}_{\mathrm{tt}}^{-1}$ the BLUE-inverse of $\mathrm{C}_{\mathrm{t}_i} = \mathrm{B}^T\mathrm{C}_i$. The PDF of $\left[\underline{\hat{\mathrm{x}}}_i^T \ \underline{\mathrm{t}}^T\right]^T$, under a $\mathcal{H}_a$, is

$$\mathcal{H}_a : \begin{bmatrix} \underline{\hat{\mathrm{x}}}_i \\ \underline{\mathrm{t}} \end{bmatrix} \sim \mathcal{N}\left(\begin{bmatrix} \mathrm{x} + \mathrm{A}^+\mathrm{R}_i\mathrm{C}_a\mathrm{b}_a \\ \mathrm{C}_{\mathrm{t}_a}\mathrm{b}_a \end{bmatrix}, \begin{bmatrix} \mathrm{Q}_{\hat{\mathrm{x}}_0\hat{\mathrm{x}}_0} + \mathrm{L}_i\mathrm{Q}_{\mathrm{tt}}\mathrm{L}_i^T & -\mathrm{L}_i\mathrm{Q}_{\mathrm{tt}} \\ -\mathrm{Q}_{\mathrm{tt}}\mathrm{L}_i^T & \mathrm{Q}_{\mathrm{tt}} \end{bmatrix} \right), \tag{11}$$

where $\mathrm{R}_i = \mathrm{I}_m - \mathrm{C}_i \left(\mathrm{B}^T \mathrm{C}_i\right)^+ \mathrm{B}^T$ projects along $\mathcal{R}(\mathrm{C}_i)$ and onto $\mathcal{R}(\mathrm{A}, \mathrm{Q}_{\mathrm{yy}}\mathrm{B}(\mathrm{B}^T\mathrm{C}_i)^{\perp})$ with $(\mathrm{B}^T\mathrm{C}_i)^{\perp}$ being a basis matrix of the null space of $\mathrm{C}_i^T\mathrm{B}$ (Teunissen, 2018). We emphasize two important cases regarding the PDF of $\left[\underline{\hat{\mathrm{x}}}_i^T \ \underline{\mathrm{t}}^T\right]^T$,

$$f_{\underline{\hat{\mathrm{x}}}_i,\underline{\mathrm{t}}}(x,t) \begin{cases} = f_{\underline{\hat{\mathrm{x}}}_0}(x) f_{\underline{\mathrm{t}}}(t) & \text{, if } i = 0 \\ \neq f_{\underline{\hat{\mathrm{x}}}_i}(x) f_{\underline{\mathrm{t}}}(t) & \text{, if } i \in \{1, ..., k\}, \end{cases} \tag{12}$$

which shows that, for $i = 0$, the BLUE $\underline{\hat{\mathrm{x}}}_0$ and the misclosure vector $\underline{\mathrm{t}}$ are independent while for $i \in \{1, ..., k\}$ the BLUEs $\underline{\hat{\mathrm{x}}}_i$ and $\underline{\mathrm{t}}$ are *dependent*.

It is possible to capture the hypothesis testing problem in (7) in the misclosure vector space $\mathbb{R}^r$ by applying partitioning principles. A partitioning of $\mathbb{R}^r$ can formulated based on $\mathcal{P}_i \subset \mathbb{R}^r$, for $i \in \{0, ..., k\}$, such that $\cup_{i=0}^{k} \mathcal{P}_i = \mathbb{R}^r$ and $\mathcal{P}_i \cap \mathcal{P}_l = \{0\}$ for $i \neq l$. Note that an undecided region $\Omega \subset \mathbb{R}^r$ could also be included to accommodate for situations when it would be difficult to discriminate between hypotheses. In this article, we consider that an estimator $\underline{\hat{\mathrm{x}}}_i$ is selected regardless of the outcome of the testing decision (i.e., no $\Omega \subset \mathbb{R}^r$ is included). The hypothesis $\mathcal{H}_i$, for $i \in \{0, ..., k\}$, is selected as the most likely one if and only if $\underline{\mathrm{t}} \in \mathcal{P}_i$, which leads to $\underline{\hat{\mathrm{x}}}_i$ to be provided as the output of the procedure. The partitions can be defined as follows

$$\mathcal{P}_0 = \left\{ t \in \mathbb{R}^r \mid ||t||^2_{\mathrm{Q}_{\mathrm{tt}}} \leq \chi^2_{\alpha}(r, 0) \right\}, \ \ \mathcal{P}_i = \left\{ t \in \mathbb{R}^r \mid t \notin \mathcal{P}_0, \ \check{\mathsf{T}}_i = \max_{l \in \{1,...,k\}} \mathsf{T}_l \right\} \text{ for } i \in \{1, ..., k\}, \tag{13}$$

where $||\underline{\mathrm{t}}||^2_{\mathrm{Q}_{\mathrm{tt}}}$ is the overall model test statistic, $\chi^2_{\alpha}(r, 0)$ is the critical value for a level of significance α, and $\underline{\mathsf{T}}_l$ is the result of the following transformation (Robert and Casella (1999); Teunissen (2017); Zaminpardaz and Teunissen (2023))

$$\underline{\mathsf{T}}_l = \mathrm{CDF}_{\chi^2(q_l,0)} \left(||\mathbf{Q}_{\mathrm{C}_{\mathrm{t}_l}} \underline{\mathrm{t}}||^2_{\mathrm{Q}_{\mathrm{tt}}} \right), \tag{14}$$

where $\mathrm{CDF}_{\chi^2(q_l,0)}(.)$ is the cumulative distribution function (CDF) of $\chi^2(q_l, 0)$, $||\mathbf{Q}_{\mathrm{C}_{\mathrm{t}_l}} \underline{\mathrm{t}}||^2_{\mathrm{Q}_{\mathrm{tt}}} \overset{\mathcal{H}_0}{\sim} \chi^2(q_l, 0)$, $\mathbf{Q}_{\mathrm{C}_{\mathrm{t}_l}} = \mathrm{C}_{\mathrm{t}_l}\mathrm{C}^+_{\mathrm{t}_l}$, and $\underline{\mathsf{T}}_l$ has a uniform distribution on the interval $[0, 1]$ under $\mathcal{H}_0$. This transformation is done such that all $\underline{\mathsf{T}}_l$'s have the same PDF under $\mathcal{H}_0$, since the dimension of the model misspecification $b_l \in \mathbb{R}^{q_l}$ generally differs across the alternative hypotheses. The maximum among them ($\check{\underline{\mathsf{T}}}_i$) corresponds to the most likely $\mathcal{H}_i$ for $i \in \{1, ..., k\}$ (Teunissen, 2017). Note that if the dimension of the model misspecification is the same across the alternative hypotheses (e.g., all equal to 1 when testing for single outliers), then the transformation step in (14) is not needed and the maximum across $||\mathbf{Q}_{\mathrm{C}_{\mathrm{t}_l}} \underline{\mathrm{t}}||^2_{\mathrm{Q}_{\mathrm{tt}}}$ can be found directly to obtain $\check{\underline{\mathsf{T}}}_i$. An example of partitioning is shown in Figure 1 for a simple datasnooping example when $\mathbb{R}^{r=2}$ (Baarda, 1968). The statistical hypothesis testing procedure can be formulated, equally, based on the BLUE's residual vector $\underline{\hat{\mathrm{e}}}_0 = \underline{\mathrm{y}} - \mathrm{A}\underline{\hat{\mathrm{x}}}_0$, which gives $\underline{\hat{\mathrm{e}}}_0 = \mathrm{Q}_{\mathrm{yy}}\mathrm{B}\,\mathrm{Q}_{\mathrm{tt}}^{-1}\underline{\mathrm{t}}$ leading to the equality of the quadratic forms $||\underline{\hat{\mathrm{e}}}_0||^2_{\mathrm{Q}_{\mathrm{yy}}} = ||\underline{\mathrm{t}}||^2_{\mathrm{Q}_{\mathrm{tt}}} \overset{\mathcal{H}_0}{\sim} \chi^2(r, 0)$ (Teunissen, 2024b).

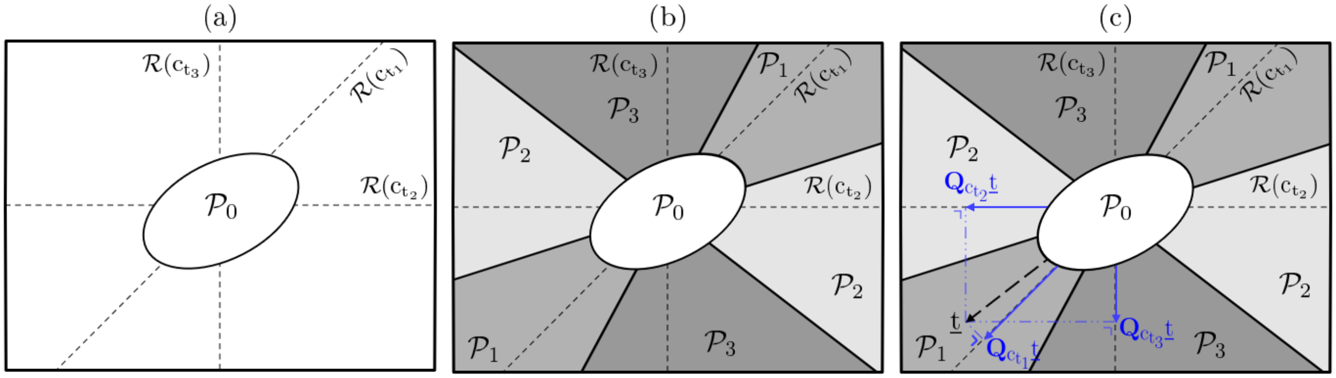

Figure 1: Partitioning of the misclosure space $\mathbb{R}^{r=2}$ when $\mathrm{x} \in \mathbb{R}$, $\mathrm{A} = [1\ 1\ 1]^T$, $\mathrm{Q}_{\mathrm{yy}} = \mathrm{I}_3$, and $\mathrm{B}^T = \begin{bmatrix} -1 & 1 & 0 \\ -1 & 0 & 1 \end{bmatrix}$. The following types of 1D model misspecifications are considered: $\mathrm{c}_1 = [1\ 0\ 0]^T$, $\mathrm{c}_2 = [0\ 1\ 0]^T$, and $\mathrm{c}_3 = [0\ 0\ 1]^T$; (a) Acceptance region $\mathcal{P}_0$ and the ranges of $\mathrm{c}_{\mathrm{t}_i} = \mathrm{B}^T\mathrm{c}_i$ for $i \in \{1, 2, 3\}$; (b) Partitions $\mathcal{P}_i = \{t \in \mathbb{R}^r \mid t \notin \mathcal{P}_0, \ |w_i| = \max_{l \in \{1,...,k\}} |w_l|\}$ with $|\underline{w}_l| = ||\mathbf{Q}_{\mathrm{c}_{\mathrm{t}_l}} \underline{\mathrm{t}}||_{\mathrm{Q}_{\mathrm{tt}}}$ being the w-test statistic (Baarda, 1968); (c) Projections of a $\underline{\mathrm{t}} \in \mathbb{R}^2$ onto the $\mathcal{R}(\mathrm{c}_{\mathrm{t}_i})$ as part of constructing the w-test statistics (in this case $|\underline{w}_1|$ is largest).

Having defined the partitions, the Detection (D) Identification (I) and Adaptation (A) procedure is

$$\begin{cases}\text{if } \underline{\mathrm{t}} \in \mathcal{P}_0 \text{ (no Detection)} \rightarrow \text{ output } \underline{\hat{\mathrm{x}}}_0,\\ \text{if } \underline{\mathrm{t}} \notin \mathcal{P}_0 \text{ (Detection)} \rightarrow \ \underline{\mathrm{t}} \in \mathcal{P}_{i\neq 0} \text{ (Identification)} \rightarrow \text{ output } \underline{\hat{\mathrm{x}}}_i \text{ (Adaptation)}.\end{cases} \tag{15}$$

It is clear that the selection of the BLUEs is dependent on where the misclosure vector $\underline{\mathrm{t}}$ lands in the partitioned $\mathbb{R}^r$. The estimator that captures *any procedure* of the form shown in (15) is the DIA-estimator (Teunissen, 2018)

$$\underline{\bar{\mathrm{x}}} = \begin{cases}\underline{\hat{\mathrm{x}}}_0, & \text{if } \underline{\mathrm{t}} \in \mathcal{P}_0\\ \underline{\hat{\mathrm{x}}}_i, & \text{if } \underline{\mathrm{t}} \in \mathcal{P}_i\end{cases} \rightarrow \quad \underline{\bar{\mathrm{x}}} = \sum_{i=0}^{k} \underline{\hat{\mathrm{x}}}_i \, p_i(\underline{\mathrm{t}}) = \underline{\hat{\mathrm{x}}}_0 - \sum_{i=1}^{k} \mathrm{L}_i \, \underline{\mathrm{t}} \, p_i(\underline{\mathrm{t}}), \tag{16}$$

where the indicator function $p_i(\underline{\mathrm{t}}) = 1$ if $\underline{\mathrm{t}} \in \mathcal{P}_i$ and 0 otherwise. The uncertainty of parameter estimation is carried by the BLUEs and the one of statistical testing is carried by $p_i(\underline{\mathrm{t}})$. Note that $p_i(\underline{\mathrm{t}})$ is a nonlinear function of $\underline{\mathrm{t}}$, which causes the PDF of the DIA-estimator $\underline{\bar{\mathrm{x}}}$ to be non-Gaussian, even though the PDFs of the BLUEs are Gaussian. Before giving the expressions for the PDF of $\underline{\bar{\mathrm{x}}}$, let us consider a 'thought experiment' to illustrate the behavior of a DIA-estimator. Consider the models from Figure 1, and assume we have access to N independent and identically distributed (i.i.d.) random samples generated from the PDF of the observables $f_{\underline{\mathrm{y}}}(y)$. Next, we execute the procedure in (15) for each random sample (see Appendix V-A for the steps to be followed). Due to the uncertainty of statistical testing carried by $p_i(\underline{\mathrm{t}})$, a possible outcome of this experiment is shown in Table 1.

Table 1: Example of possible outcome of a combined parameter estimation and statistical hypothesis testing procedure (Appendix V-A).

Nb.	1	2	3	4	...	N
Statistical testing decision	$\underline{\mathrm{t}} \in \mathcal{P}_3$	$\underline{\mathrm{t}} \in \mathcal{P}_1$	$\underline{\mathrm{t}} \in \mathcal{P}_0$	$\underline{\mathrm{t}} \in \mathcal{P}_2$	...	$\underline{\mathrm{t}} \in \mathcal{P}_1$
Outcome of $\underline{\bar{\mathrm{x}}}$	$\hat{\mathrm{x}}_3$	$\hat{\mathrm{x}}_1$	$\hat{\mathrm{x}}_0$	$\hat{\mathrm{x}}_2$	...	$\hat{\mathrm{x}}_1$

In positioning safety analyses one should consider the distribution of $\underline{\bar{\mathrm{x}}}$ instead that of the individual BLUEs $\underline{\hat{\mathrm{x}}}_i$. If we would consider only the BLUEs $\underline{\hat{\mathrm{x}}}_i$ and their PDFs in positioning safety analyses we would *wrongfully* discard the uncertainty associated to statistical testing. The PDF of $\underline{\bar{\mathrm{x}}}$ follows from Theorem 1 in (Teunissen, 2018)

$$f_{\underline{\bar{\mathrm{x}}}}(x) = f_{\underline{\hat{\mathrm{x}}}_0}(x) \int_{\mathcal{P}_0} f_{\underline{\mathrm{t}}}(t)dt + \sum_{i=0}^{k} \int_{\mathcal{P}_i} f_{\underline{\hat{\mathrm{x}}}_i,\underline{\mathrm{t}}}(x,t)\,dt = f_{\underline{\hat{\mathrm{x}}}_0}(x) \int_{\mathcal{P}_0} f_{\underline{\mathrm{t}}}(t)dt + \sum_{i=1}^{k} \int_{\mathcal{P}_i} f_{\underline{\hat{\mathrm{x}}}_0}(x + \mathrm{L}_i\, t)\, f_{\underline{\mathrm{t}}}(t)dt, \tag{17}$$

where use has been made of the equality $f_{\underline{\hat{\mathrm{x}}}_0,\underline{\mathrm{t}}}(x,t) = f_{\underline{\hat{\mathrm{x}}}_0}(x) f_{\underline{\mathrm{t}}}(t)$ for $i = 0$ from (12). In (17) we see that the number of total hypotheses $k+1$, the partitions $\mathcal{P}_i \subset \mathbb{R}^r$, and the joint PDFs $f_{\underline{\hat{\mathrm{x}}}_i,\underline{\mathrm{t}}}(x,t)$, for $i \in \{0,...,k\}$, constitute the required elements to construct $f_{\underline{\bar{\mathrm{x}}}}(x)$. Therefore, changes in any of these elements will be reflected in $f_{\underline{\bar{\mathrm{x}}}}(x)$. Considering the statistical testing decisions $\mathcal{H}_0$, such as CA and FA, use can be made of the rule of total probability to decompose (17) as follows

$$f_{\underline{\bar{\mathrm{x}}}}(x|\mathcal{H}_0) = \mathsf{P}_{\mathrm{CA}} f_{\underline{\bar{\mathrm{x}}}|\mathrm{CA}}(x|\mathrm{CA}) + \sum_{j=1}^{k} \mathsf{P}_{\mathrm{FA}_j} f_{\underline{\bar{\mathrm{x}}}|\mathrm{FA}_j}(x|\mathrm{FA}_j) \ \text{ with } f_{\underline{\bar{\mathrm{x}}}|\mathrm{FA}_j}(x|\mathrm{FA}_j) = \frac{\int_{\mathcal{P}_j} f_{\underline{\hat{\mathrm{x}}}_j,\underline{\mathrm{t}}}(x,t|\mathcal{H}_0)\,dt}{\mathsf{P}_{\mathrm{FA}_j}}, \tag{18}$$

where $f_{\underline{\bar{\mathrm{x}}}|\mathrm{CA}}(x|\mathrm{CA}) = f_{\underline{\hat{\mathrm{x}}}_0}(x|\mathcal{H}_0)$ with $f_{\underline{\hat{\mathrm{x}}}_0}(x|\mathcal{H}_0) = \mathcal{N}(\mathrm{x}, \mathrm{Q}_{\hat{\mathrm{x}}_0\hat{\mathrm{x}}_0})$, and $\mathsf{P}_{\mathrm{CA}} = \mathsf{P}(\underline{\mathrm{t}} \in \mathcal{P}_0|\mathcal{H}_0)$, $\mathsf{P}_{\mathrm{FA}_j} = \mathsf{P}(\underline{\mathrm{t}} \in \mathcal{P}_j|\mathcal{H}_0)$ are the probabilities of the respective events. The summation term in (18) causes $f_{\underline{\bar{\mathrm{x}}}}(x|\mathcal{H}_0)$ to be a nonnormal PDF. Similarly, under an alternative $\mathcal{H}_i$ for $i \neq 0$, the decomposition of (17) gives

$$f_{\underline{\bar{\mathrm{x}}}}(x|\mathcal{H}_i) = \mathsf{P}_{\mathrm{MD}_i} f_{\underline{\bar{\mathrm{x}}}|\mathrm{MD}_i}(x|\mathrm{MD}_i) + \mathsf{P}_{\mathrm{CI}_i} f_{\underline{\bar{\mathrm{x}}}|\mathrm{CI}_i}(x|\mathrm{CI}_i) + \sum_{j\neq 0,i}^{k} \mathsf{P}_{\mathrm{WI}_j} f_{\underline{\bar{\mathrm{x}}}|\mathrm{WI}_j}(x|\mathrm{WI}_j), \tag{19}$$

where $f_{\underline{\bar{\mathrm{x}}}|\mathrm{MD}_i}(x|\mathrm{MD}_i) = f_{\underline{\hat{\mathrm{x}}}_0}(x|\mathcal{H}_i)$ with $f_{\underline{\hat{\mathrm{x}}}_0}(x|\mathcal{H}_i) = \mathcal{N}(\mathrm{x} + \mathrm{A}^+\mathrm{C}_i\mathrm{b}_i, \mathrm{Q}_{\hat{\mathrm{x}}_0\hat{\mathrm{x}}_0})$, and $\mathsf{P}_{\mathrm{MD}_i} = \mathsf{P}(\underline{\mathrm{t}} \in \mathcal{P}_0|\mathcal{H}_i)$, $\mathsf{P}_{\mathrm{CI}_i} = \mathsf{P}(\underline{\mathrm{t}} \in \mathcal{P}_i|\mathcal{H}_i)$, $\mathsf{P}_{\mathrm{WI}_j} = \mathsf{P}(\underline{\mathrm{t}} \in \mathcal{P}_j|\mathcal{H}_i)$ are the probabilities of the respective events. The expressions of the individual components under CI_i and WI_j are

$$f_{\underline{\bar{\mathrm{x}}}|\mathrm{CI}_i}(x|\mathrm{CI}_i) = \frac{\int_{\mathcal{P}_i} f_{\underline{\hat{\mathrm{x}}}_i,\underline{\mathrm{t}}}(x,t|\mathcal{H}_i)\,dt}{\mathsf{P}_{\mathrm{CI}_i}}, \ f_{\underline{\bar{\mathrm{x}}}|\mathrm{WI}_j}(x|\mathrm{WI}_j) = \frac{\int_{\mathcal{P}_j} f_{\underline{\hat{\mathrm{x}}}_j,\underline{\mathrm{t}}}(x,t|\mathcal{H}_j)\,dt}{\mathsf{P}_{\mathrm{WI}_j}}. \tag{20}$$

In (19) the PDF $f_{\overline{\underline{x}}}\,(x|\mathcal{H}_i)$ is nonnormal due to the second and third terms. To compute $f_{\overline{\underline{x}}}\,(x|\mathcal{H}_i)$, and/or its components, one would need to set or make assumptions on the size of the model misspecification $\mathrm{b}_i \in \mathbb{R}^{q_i}$. The PDFs discussed in this section form the basis for expressing the probabilities of positioning failure in the next section.

III. PROBABILITY OF POSITIONING FAILURE AND ITS COMPONENTS

The *probability of positioning failure* is formulated based on the event of positioning failure $\mathcal{F} = \{\overline{\underline{x}} \in \mathcal{B}^c\}$ (page 15 in (RTCA-Special Committee 159, 2020)) and on the DIA-estimator's PDF from (17). The expression for the probability of positioning failure and its components is provided below

$$\begin{aligned}
\mathbb{P}_{\mathcal{F}}(\mathbf{b}) &= \mathsf{P}(\mathcal{H}_0)\,\mathbb{P}_{\mathcal{F}}|\mathcal{H}_0 + \sum_{i=1}^{k}\mathsf{P}(\mathcal{H}_i)\,\mathbb{P}_{\mathcal{F}}|\mathcal{H}_i(\mathrm{b}_i)\\
&= \mathsf{P}(\mathcal{H}_0)\int_{\mathcal{B}^c} f_{\overline{\underline{x}}}(x|\mathcal{H}_0)dx + \sum_{i=1}^{k}\mathsf{P}(\mathcal{H}_i)\int_{\mathcal{B}^c} f_{\overline{\underline{x}}}(x|\mathcal{H}_i)dx\\
&= \mathsf{P}(\mathcal{H}_0)\left(\sum_{j=0}^{k}\int_{\mathcal{B}^c}\int_{\mathcal{P}_j} f_{\hat{\underline{x}}_j,\underline{t}}\,(x,t|\mathcal{H}_0)\,dt\,dx\right) + \sum_{i=1}^{k}\mathsf{P}(\mathcal{H}_i)\left(\sum_{j=0}^{k}\int_{\mathcal{B}^c}\int_{\mathcal{P}_j} f_{\hat{\underline{x}}_j,\underline{t}}\,(x,t|\mathcal{H}_i)\,dt\,dx\right)\\
&= \mathsf{P}(\mathcal{H}_0)\left(\sum_{j=0}^{k}\mathsf{E}_{f_{\hat{\underline{x}}_j,\underline{t}}}\,(\mathbb{1}_j(\underline{x},\underline{t})|\mathcal{H}_0)\right) + \sum_{i=1}^{k}\mathsf{P}(\mathcal{H}_i)\left(\sum_{j=0}^{k}\mathsf{E}_{f_{\hat{\underline{x}}_j,\underline{t}}}\,(\mathbb{1}_j(\underline{x},\underline{t})|\mathcal{H}_i)\right),
\end{aligned} \tag{21}$$

where the dependence on the model misspecifications is accounted in the notation of $\mathbb{P}_{\mathcal{F}}(\mathbf{b})$ with $\mathbf{b} = \{\mathrm{b}_1, ..., \mathrm{b}_k\}$, $\mathcal{B}^c = \mathbb{R}^n \backslash \mathcal{B}$ is the failure-region (complement of the safety-region $\mathcal{B} \subset \mathbb{R}^n$), and the joint indicator function $\mathbb{1}_j(\underline{x},\underline{t}) = 1$ if $[\underline{x}^T\ \underline{t}^T]^T \in (\mathcal{B}^c \cap \mathcal{P}_j)$, and 0 otherwise. The summation terms in parentheses in the last line of (21) are denoted below, taking into account the statistical testing decisions in the notation,

$$\begin{cases}\sum_{j=0}^{k}\mathsf{E}_{f_{\hat{\underline{x}}_j,\underline{t}}}\,(\mathbb{1}_j(\underline{x},\underline{t})|\mathcal{H}_0) = \mathbb{P}_{\mathcal{F}}|\mathrm{CA}\,\mathsf{P}_{\mathrm{CA}} + \sum_{j=1}^{k}\mathbb{P}_{\mathcal{F}}|\mathrm{FA}_j\,\mathsf{P}_{\mathrm{FA}_j},\\ \sum_{j=0}^{k}\mathsf{E}_{f_{\hat{\underline{x}}_j,\underline{t}}}\,(\mathbb{1}_j(\underline{x},\underline{t})|\mathcal{H}_i) = \mathbb{P}_{\mathcal{F}}|\mathrm{MD}_i\,\mathsf{P}_{\mathrm{MD}_i} + \mathbb{P}_{\mathcal{F}}|\mathrm{CI}_i\,\mathsf{P}_{\mathrm{CI}_i} + \sum_{j\neq 0,i}^{k}\mathbb{P}_{\mathcal{F}}|\mathrm{WI}_j\,\mathsf{P}_{\mathrm{WI}_j}\ .\end{cases} \tag{22}$$

The decompositions from (21) and (22) are illustrated schematically in Figure 2. By computing (22) one can obtain a complete picture over the components that are the most or least influential to $\mathbb{P}_{\mathcal{F}}|\mathcal{H}_0$ and/or to $\mathbb{P}_{\mathcal{F}}|\mathcal{H}_i(\mathrm{b}_i)$. Knowledge about the MICs and/or LICs of $\mathbb{P}_{\mathcal{F}}|\mathcal{H}_0$ and/or of $\mathbb{P}_{\mathcal{F}}|\mathcal{H}_i(\mathrm{b}_i)$ can be valuable at the design stages of the algorithms for parameter estimation and statistical hypothesis testing. Note that at this stage, the MICs and LICs are intrinsic to the designed DIA-estimator and do not depend on the 'weighting' given by the a-priori probabilities.

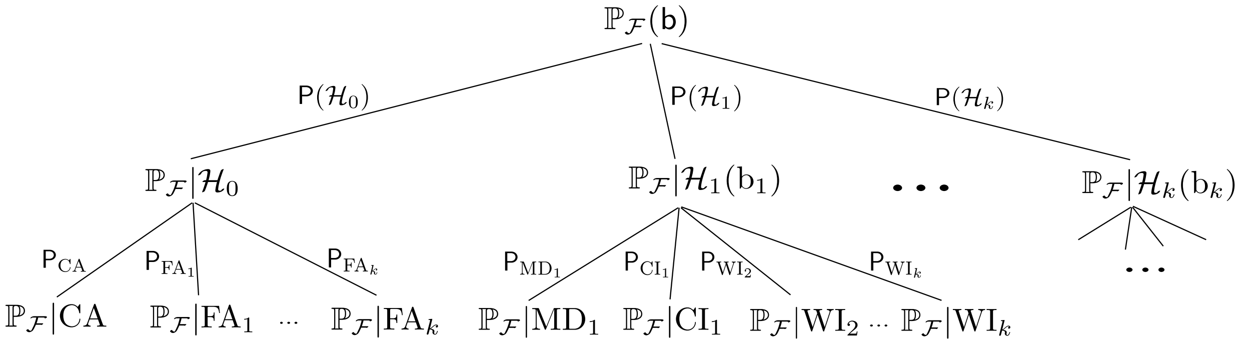

Figure 2: Schematic representation of the conditional components of $\mathbb{P}_{\mathcal{F}}(\mathbf{b})$.

For positioning safety analyses, the maximum of (21) can be compared against an application specific requirement to decide whether the requirement is met,

$$\max_{\mathbf{b}} \mathbb{P}_{\mathcal{F}}(\mathbf{b}) = \mathsf{P}(\mathcal{H}_0)\mathbb{P}_{\mathcal{F}|\mathcal{H}_0} + \max_{\mathrm{b}_1,\ldots,\mathrm{b}_k} \sum_{i=1}^{k} \mathsf{P}(\mathcal{H}_i)\mathbb{P}_{\mathcal{F}|\mathcal{H}_i}(\mathrm{b}_i). \tag{23}$$

The positioning safety-analyses in the next section are based on constructing the 'failure-tree' shown in Figure 2.

IV. POSITIONING SAFETY ANALYSES

1. One-dimensional positioning example

To illustrate the principles from the previous sections, we make use of a simple one-dimensional positioning example where we assume $\underline{\mathrm{y}} = [\underline{y}_1 \;\; \underline{y}_2]^T \in \mathbb{R}^2$, $\underline{\mathrm{y}} \sim \mathcal{N}(\mathsf{E}_{f_{\underline{\mathrm{y}}}}(\underline{\mathrm{y}}), \mathrm{Q_{yy}})$, and the to-be-estimated unknown scalar $\mathrm{x} \in \mathbb{R}$ in [m]. This choice is made such that the integration regions in the joint-vector space $\mathbb{R}^{(n+r)}$ can be visualized. In this case $m = 2$ and $n = r = k = 1$ based on which the following statistical hypothesis testing problem is formulated

$$\mathcal{H}_0 : \mathsf{E}_{f_{\underline{\mathrm{y}}}}\left(\underline{\mathrm{y}}\right) = \mathrm{Ax} \quad \text{vs.} \quad \mathcal{H}_1 : \mathsf{E}_{f_{\underline{\mathrm{y}}}}\left(\underline{\mathrm{y}}\right) = \mathrm{Ax} + \mathrm{c}_1\mathrm{b}_1, \tag{24}$$

with $\mathrm{Q_{yy}} = \sigma_{\mathrm{y}}^2 \mathrm{I}_2$ [m^2], $\mathrm{A} = [1 \quad 1]^T$, $\mathrm{B}^T = [1 \quad -1]$, $\mathrm{c}_1 = [1 \quad 0]^T$, $\mathrm{c}_{\mathrm{t}_1} = \mathrm{B}^T\mathrm{c}_1 = 1$, and $\mathrm{b}_1 \in \mathbb{R}$ in [m]. It follows that $\mathrm{Q}_{\hat{\mathrm{x}}_0\hat{\mathrm{x}}_0} = \sigma_{\hat{\mathrm{x}}_0}^2 = 0.5\,\sigma_{\mathrm{y}}^2$ [m^2] and $\mathrm{Q_{tt}} = \sigma_{\mathrm{t}}^2 = 2\,\sigma_{\mathrm{y}}^2$ [m^2]. The PDF of $[\underline{\hat{\mathrm{x}}}_i \;\; \underline{\mathrm{t}}]^T \in \mathbb{R}^2$ under $\mathcal{H}_0$ and $\mathcal{H}_1$ is

$$\mathcal{H}_0 : \begin{bmatrix} \underline{\hat{\mathrm{x}}}_i \\ \underline{\mathrm{t}} \end{bmatrix} \sim \mathcal{N}\left(\begin{bmatrix} \mathrm{x} \\ 0 \end{bmatrix}, \begin{bmatrix} \sigma_{\hat{\mathrm{x}}_0}^2 + \mathrm{L}_i^2\sigma_{\mathrm{t}}^2 & -\mathrm{L}_i\sigma_{\mathrm{t}}^2 \\ -\mathrm{L}_i\sigma_{\mathrm{t}}^2 & \sigma_{\mathrm{t}}^2 \end{bmatrix} \right), \quad \mathcal{H}_1 : \begin{bmatrix} \underline{\hat{\mathrm{x}}}_i \\ \underline{\mathrm{t}} \end{bmatrix} \sim \mathcal{N}\left(\begin{bmatrix} \mathrm{x} + \mathrm{A}^+\mathrm{R}_i\mathrm{c}_1\mathrm{b}_1 \\ \mathrm{b}_1 \end{bmatrix}, \begin{bmatrix} \sigma_{\hat{\mathrm{x}}_0}^2 + \mathrm{L}_i^2\sigma_{\mathrm{t}}^2 & -\mathrm{L}_i\sigma_{\mathrm{t}}^2 \\ -\mathrm{L}_i\sigma_{\mathrm{t}}^2 & \sigma_{\mathrm{t}}^2 \end{bmatrix} \right) \tag{25}$$

for $i \in \{0, 1\}$, where $\mathrm{L}_0 = 0$, $\mathrm{L}_1 = \mathrm{A}^+\mathrm{c}_1\mathrm{c}_{\mathrm{t}_1}^+ = 0.5$, $\mathrm{A}^+ = [0.5 \quad 0.5]$, $\mathrm{R}_0 = \mathrm{I}_2$, and $\mathrm{R}_1 = \begin{bmatrix} 0 & 1 \\ 0 & 1 \end{bmatrix}$. The correlation coefficient between $\underline{\hat{\mathrm{x}}}_1$ and $\underline{\mathrm{t}}$ is

$$\rho_{\underline{\hat{\mathrm{x}}}_1,\underline{\mathrm{t}}} = -\frac{\mathrm{L}_1\sigma_{\mathrm{t}}}{\sqrt{\sigma_{\hat{\mathrm{x}}_0}^2 + \mathrm{L}_1^2\sigma_{\mathrm{t}}^2}} = -\frac{\sqrt{2}}{2}. \tag{26}$$

If different models would have been chosen (e.g., different A, $\mathrm{Q_{yy}}$, c_1), then $\rho_{\underline{\hat{\mathrm{x}}}_1,\underline{\mathrm{t}}}$ would be different (see Appendix V-B). The partitioning of the misclosure space in $\mathbb{R}$ for a chosen $\alpha = \mathsf{P}_{\mathsf{FA}}$ gives,

$$\mathcal{P}_0 = \left\{ t \in \mathbb{R} \mid -\tau_{\frac{\alpha}{2}}\sigma_{\mathrm{t}} \leq t \leq \tau_{\frac{\alpha}{2}}\sigma_{\mathrm{t}} \right\}, \quad \mathcal{P}_1 = \mathbb{R}/\mathcal{P}_0, \tag{27}$$

where $\tau_{\frac{\alpha}{2}}$ is the critical value. When $k = 1$ there are four hypothesis testing decisions: CA ($\underline{\mathrm{t}} \in \mathcal{P}_0|\mathcal{H}_0$), FA ($\underline{\mathrm{t}} \notin \mathcal{P}_0|\mathcal{H}_0$), MD$_1$ ($\underline{\mathrm{t}} \in \mathcal{P}_0|\mathcal{H}_1$), and Correct Detection-CD$_1$ ($\underline{\mathrm{t}} \notin \mathcal{P}_0|\mathcal{H}_1$). Next we define the safety-region in the parameter space $\mathbb{R}$ to be an interval centred at the true value x,

$$\mathcal{B} = \{ x \in \mathbb{R} \mid \mathrm{x} - \beta \leq x \leq \mathrm{x} + \beta \}, \tag{28}$$

for a chosen positive value β.

The PDF $f_{\underline{\bar{\mathrm{x}}}}(x|\mathcal{H}_0)$, its conditional components ($f_{\underline{\bar{\mathrm{x}}}|\mathrm{CA}}(x|\mathrm{CA})$ and $f_{\underline{\bar{\mathrm{x}}}|\mathrm{FA}}(x|\mathrm{FA})$), and the interval $\mathcal{B}$ are shown in Figure 3(a). From (18) and (25) it follows that $f_{\underline{\bar{\mathrm{x}}}|\mathrm{CA}}(x|\mathrm{CA}) = f_{\underline{\hat{\mathrm{x}}}_0}(x|\mathcal{H}_0) = \mathcal{N}\left(\mathrm{x}, \sigma_{\hat{\mathrm{x}}_0}^2\right)$. The shape of $f_{\underline{\bar{\mathrm{x}}}|\mathrm{FA}}(x|\mathrm{FA})$ can be explained starting from its expression in (18)

$$f_{\underline{\bar{\mathrm{x}}}|\mathrm{FA}}(x|\mathrm{FA}) = \frac{1}{\mathsf{P}_{\mathsf{FA}}}\left(\int_{-\infty}^{-\tau_{\frac{\alpha}{2}}\sigma_{\mathrm{t}}} f_{\underline{\hat{\mathrm{x}}}_0}\left(x + \mathrm{L}_1 t|\mathcal{H}_0\right) f_{\underline{\mathrm{t}}}(t|\mathcal{H}_0)dt + \int_{\tau_{\frac{\alpha}{2}}\sigma_{\mathrm{t}}}^{\infty} f_{\underline{\hat{\mathrm{x}}}_0}\left(x + \mathrm{L}_1 t|\mathcal{H}_0\right) f_{\underline{\mathrm{t}}}(t|\mathcal{H}_0)dt \right), \tag{29}$$

where the two terms in the sum give two modes due to the symmetry of $f_{\underline{\mathrm{t}}}(t|\mathcal{H}_0)$ w.r.t. the origin and $\mathcal{P}_0$. Assuming σ_{y} is fixed, if $\mathsf{P}_{\mathsf{FA}} \downarrow$ then the interval $\mathcal{P}_0 \uparrow$ and the distance between the two modes increases which leads to $f_{\underline{\bar{\mathrm{x}}}}(x|\mathcal{H}_0)$ to approach $f_{\underline{\bar{\mathrm{x}}}|\mathrm{CA}}(x|\mathrm{CA})$. Conversely, if $\mathsf{P}_{\mathsf{FA}} \uparrow$, then $\mathcal{P}_0 \downarrow$ and the distance between the two modes decreases which results in a $f_{\underline{\bar{\mathrm{x}}}}(x|\mathcal{H}_0)$ with heavier tails. For a fixed P_{FA} and an increasing precision of the observables $\underline{\mathrm{y}}$ ($\sigma_{\mathrm{y}} \downarrow$), and consequently a higher precision of $\underline{\mathrm{t}}$ ($\sigma_{\mathrm{t}} \downarrow$) and $\underline{\hat{\mathrm{x}}}_0$ ($\sigma_{\hat{\mathrm{x}}_0} \downarrow$), the modes would become narrower and get closer to one another. Conversely, with poorer precision ($\sigma_{\mathrm{t}} \uparrow$, $\sigma_{\hat{\mathrm{x}}_0} \uparrow$), the modes would be wider and further apart. In these situations the width of $f_{\underline{\bar{\mathrm{x}}}}(x|\mathcal{H}_0)$ and its two components

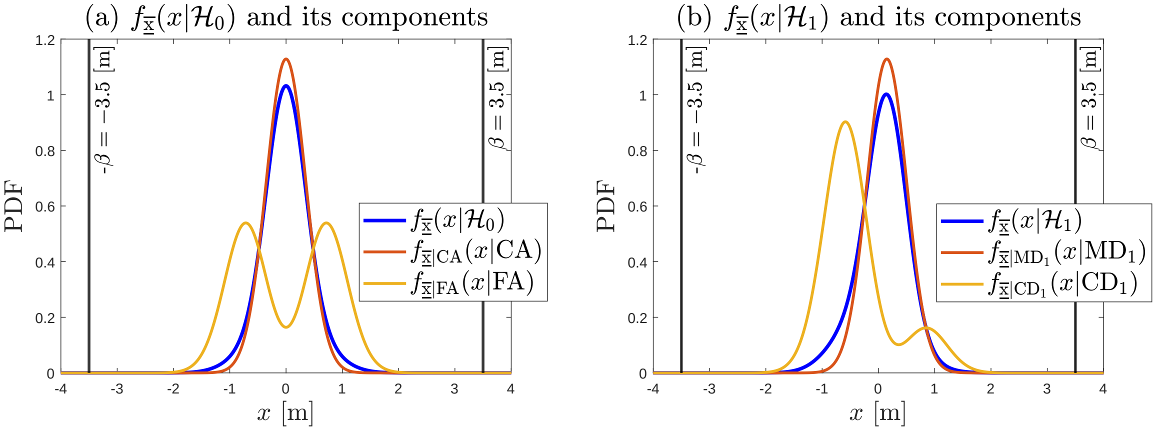
(a) $f_{\underline{\mathrm{x}}}(x|\mathcal{H}_0)$ and its components

(b) $f_{\underline{\mathrm{x}}}(x|\mathcal{H}_1)$ and its components

Figure 3: The following parameters have been used for illustration purposes: $\mathrm{x} = 0$, $\beta = 3.5$ [m], $\sigma_{\mathrm{y}}^2 = 0.250$ [m^2], $\sigma_{\hat{\mathrm{x}}_0}^2 = 0.125$ [m^2], $\sigma_{\mathrm{t}}^2 = 0.500$ [m^2], and for (a) $\mathcal{H}_0 : \alpha = \mathsf{P}_{\mathrm{FA}} = 0.1$, $\mathsf{P}_{\mathrm{CA}} = 0.9$; (b) $\mathcal{H}_1 : \mathrm{b}_1 = 0.300$ [m], $\mathrm{b}_{\hat{\mathrm{x}}_0} = \mathrm{A}^+\mathrm{c}_1\mathrm{b}_1 = 0.150$ [m], $\mathrm{b}_{\mathrm{t}} = \mathrm{b}_1$, $\mathsf{P}_{\mathrm{MD}_1} = 0.8696$, and $\mathsf{P}_{\mathrm{CD}_1} = 0.1304$.

would vary in accordance to σ_{y}.

For $f_{\underline{\mathrm{x}}}(x|\mathcal{H}_1)$ one would need to make assumptions on the value of the model misspecification, in this case the outlier b_1, to carry out a similar analysis. An example is shown in Figure 3(b) for $\mathrm{b}_1 = 0.3$ [m]. From (19) and (25) it follows that $f_{\underline{\mathrm{x}}|\mathrm{MD}_1}(x|\mathrm{MD}_1) = f_{\hat{\underline{\mathrm{x}}}_0}(x|\mathcal{H}_1) = \mathcal{N}\left(\mathrm{x} + \mathrm{A}^+\mathrm{c}_1\mathrm{b}_1, \sigma_{\hat{\mathrm{x}}_0}^2\right)$. The shape of $f_{\underline{\mathrm{x}}|\mathrm{CD}_1}(x|\mathrm{CD}_1)$ can be explained starting from its expression

$$f_{\underline{\mathrm{x}}|\mathrm{CD}_1}(x|\mathrm{CD}_1) = \frac{1}{\mathsf{P}_{\mathrm{CD}_1}}\left(\int_{-\infty}^{-\tau_{\frac{\alpha}{2}}\sigma_{\mathrm{t}}} f_{\hat{\underline{\mathrm{x}}}_0}\left(x + \mathrm{L}_1 t|\mathcal{H}_1\right) f_{\underline{\mathrm{t}}}(t|\mathcal{H}_1)dt + \int_{\tau_{\frac{\alpha}{2}}\sigma_{\mathrm{t}}}^{\infty} f_{\hat{\underline{\mathrm{x}}}_0}\left(x + \mathrm{L}_1 t|\mathcal{H}_1\right) f_{\underline{\mathrm{t}}}(t|\mathcal{H}_1)dt\right), \tag{30}$$

where the smaller mode corresponds to the first term in the sum since $f_{\underline{\mathrm{t}}}(t|\mathcal{H}_1)$ is *not* symmetric w.r.t. the origin and $\mathcal{P}_0$, which means that, in the misclosure space $\mathbb{R}$, there is less density on the interval $\left(-\infty, -\tau_{\frac{\alpha}{2}}\sigma_{\mathrm{t}}\right]$ than on $\left[\tau_{\frac{\alpha}{2}}\sigma_{\mathrm{t}}, \infty\right)$. The larger mode corresponds to the second term in the sum. By keeping b_1 and σ_{y} fixed, and reducing $\mathsf{P}_{\mathrm{FA}} \downarrow$, the two modes would increasingly diverge in location, with the smaller one progressively diminishing as $\mathcal{P}_0 \uparrow$. This behavior will cause $f_{\underline{\mathrm{x}}}(x|\mathcal{H}_1)$ to approach $f_{\underline{\mathrm{x}}|\mathrm{MD}_1}(x|\mathrm{MD}_1)$, while for $\mathsf{P}_{\mathrm{FA}} \uparrow$ it would approach $f_{\hat{\underline{\mathrm{x}}}_1}(x|\mathcal{H}_1)$. In terms of a higher or poorer precision of the observations ($\sigma_{\mathrm{y}} \downarrow\uparrow \rightarrow \sigma_{\hat{\mathrm{x}}_0} \downarrow\uparrow,\ \sigma_{\mathrm{t}} \downarrow\uparrow$), the width of $f_{\underline{\mathrm{x}}}(x|\mathcal{H}_1)$ and its two components would vary accordingly. If $b_1 \uparrow$, when P_{FA} and σ_{y} are fixed, the smaller mode would diminish, which would cause $f_{\underline{\mathrm{x}}}(x|\mathcal{H}_1)$ to approach $f_{\hat{\underline{\mathrm{x}}}_1}(x|\mathcal{H}_1)$. For negative values for the model outliers, the shape and behaviour of the two modes would have been the other way around.

We now decompose the total probability of the one-dimensional positioning failure

$$\begin{aligned}
\mathbb{P}_{\mathcal{F}}(\mathrm{b}_1) &= \mathsf{P}(\mathcal{H}_0)\mathbb{P}_{\mathcal{F}}|\mathcal{H}_0 + \mathsf{P}(\mathcal{H}_1)\mathbb{P}_{\mathcal{F}}|\mathcal{H}_1(\mathrm{b}_1) \\
&= \left(\mathsf{P}_{\mathrm{CA}}\mathbb{P}_{\mathcal{F}}|\mathrm{CA} + \mathsf{P}_{\mathrm{FA}}\mathbb{P}_{\mathcal{F}}|\mathrm{FA}\right)\mathsf{P}(\mathcal{H}_0) + \left(\mathsf{P}_{\mathrm{MD}_1}\mathbb{P}_{\mathcal{F}}|\mathrm{MD}_1 + \mathsf{P}_{\mathrm{CD}_1}\mathbb{P}_{\mathcal{F}}|\mathrm{CD}_1\right)\mathsf{P}(\mathcal{H}_1) \\
&= \left(\mathsf{E}_{f_{\hat{\underline{\mathrm{x}}}_0,\underline{\mathrm{t}}}}\left(\mathbb{1}_0(\underline{\mathrm{x}},\underline{\mathrm{t}})|\mathcal{H}_0\right) + \mathsf{E}_{f_{\hat{\underline{\mathrm{x}}}_1,\underline{\mathrm{t}}}}\left(\mathbb{1}_1(\underline{\mathrm{x}},\underline{\mathrm{t}})|\mathcal{H}_0\right)\right)\mathsf{P}(\mathcal{H}_0) + \left(\mathsf{E}_{f_{\hat{\underline{\mathrm{x}}}_0,\underline{\mathrm{t}}}}\left(\mathbb{1}_0(\underline{\mathrm{x}},\underline{\mathrm{t}})|\mathcal{H}_1\right) + \mathsf{E}_{f_{\hat{\underline{\mathrm{x}}}_1,\underline{\mathrm{t}}}}\left(\mathbb{1}_1(\underline{\mathrm{x}},\underline{\mathrm{t}})|\mathcal{H}_1\right)\right)\mathsf{P}(\mathcal{H}_1).
\end{aligned} \tag{31}$$

The expected values in (31) are the integrals of $f_{\hat{\underline{\mathrm{x}}}_i,\underline{\mathrm{t}}}(x,t)$ (under $\mathcal{H}_0$ and $\mathcal{H}_1$), for $i \in \{0,1\}$, over the regions

$$\mathcal{B}^c \cap \mathcal{P}_0 = \left\{[x\ \ t]^T \in \mathbb{R}^2 \mid x \in \mathcal{B}^c,\ t \in \mathcal{P}_0\right\}\ \ ,\ \ \mathcal{B}^c \cap \mathcal{P}_1 = \left\{[x\ \ t]^T \in \mathbb{R}^2 \mid x \in \mathcal{B}^c,\ t \in \mathcal{P}_1\right\}, \tag{32}$$

which are illustrated in Figure 4. The region $(\mathcal{B}^c \cap \mathcal{P}_0) \subset \mathbb{R}^2$ has two unbounded and disjoint components, while $(\mathcal{B}^c \cap \mathcal{P}_1) \subset \mathbb{R}^2$ has four. The contour lines in Figure 4(a) and (c) correspond to the joint PDF $f_{\hat{\underline{\mathrm{x}}}_0,\underline{\mathrm{t}}}(x,t)$ under $\mathcal{H}_0$ and $\mathcal{H}_1$ while in Figure 4(b) and (d) correspond to $f_{\hat{\underline{\mathrm{x}}}_1,\underline{\mathrm{t}}}(x,t)$ under $\mathcal{H}_0$ and $\mathcal{H}_1$.

The results of the computed terms $\mathsf{P}_{\mathrm{CA}}\underline{\mathbb{P}}_{\mathcal{F}}|\mathrm{CA}$, $\underline{\mathsf{P}}_{\mathrm{FA}}\underline{\mathbb{P}}_{\mathcal{F}}|\mathrm{FA}$, $\mathsf{P}_{\mathrm{MD}_1}\underline{\mathbb{P}}_{\mathcal{F}}|\mathrm{MD}_1$, and $\underline{\mathsf{P}}_{\mathrm{CD}_1}\underline{\mathbb{P}}_{\mathcal{F}}|\mathrm{CD}_1$ are shown in Figure 5. Figure 5(a) shows the results over $N_{\mathrm{sim}} = 100$ (number of independent simulation repetitions) of $\mathsf{P}_{\mathrm{CA}}\underline{\mathbb{P}}_{\mathcal{F}}|\mathrm{CA}$ and $\underline{\mathsf{P}}_{\mathrm{FA}}\underline{\mathbb{P}}_{\mathcal{F}}|\mathrm{FA}$,

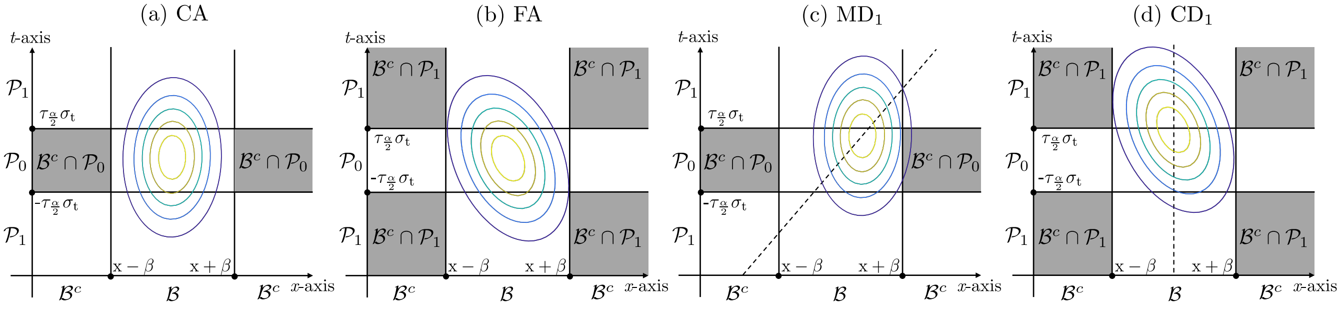

Figure 4: The grey areas illustrate the regions of integrating: (a) $f_{\underline{\hat{\mathrm{x}}}_0,\underline{\mathrm{t}}}(x,t|\mathcal{H}_0)$ over $\mathcal{B}^c\cap\mathcal{P}_0$; (b) $f_{\underline{\hat{\mathrm{x}}}_1,\underline{\mathrm{t}}}(x,t|\mathcal{H}_0)$ over $\mathcal{B}^c\cap\mathcal{P}_1$; (c) $f_{\underline{\hat{\mathrm{x}}}_0,\underline{\mathrm{t}}}(x,t|\mathcal{H}_1)$ over $\mathcal{B}^c\cap\mathcal{P}_0$, and the dashed line is the trajectory along which $f_{\underline{\hat{\mathrm{x}}}_0,\underline{\mathrm{t}}}(x,t|\mathcal{H}_1)$ moves as a function of b_1; (d) $f_{\underline{\hat{\mathrm{x}}}_1,\underline{\mathrm{t}}}(x,t|\mathcal{H}_1)$ over $\mathcal{B}^c\cap\mathcal{P}_1$, and the dashed line is the trajectory along which $f_{\underline{\hat{\mathrm{x}}}_1,\underline{\mathrm{t}}}(x,t|\mathcal{H}_1)$ moves as a function of b_1.

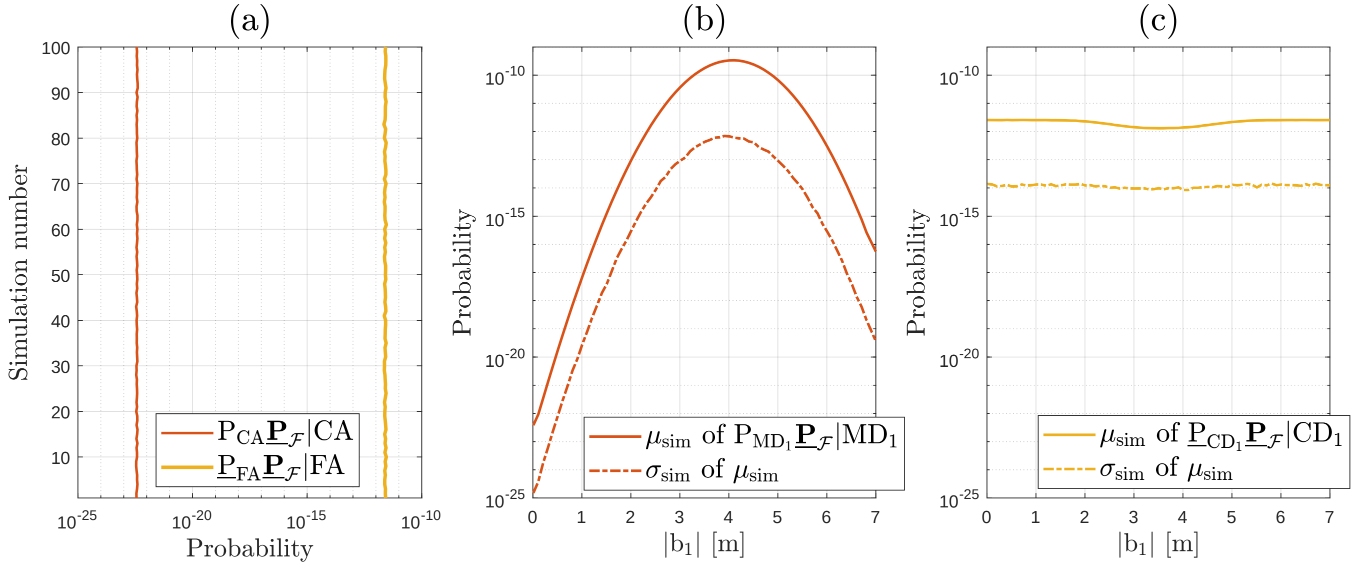

Figure 5: The following parameters have been used: $\mathrm{x}=0$, $\beta=3.5$ [m], $\sigma_{\mathrm{y}}^2=0.250$ [m^2], $\sigma_{\hat{\mathrm{x}}_0}^2=0.125$ [m^2], $\sigma_{\mathrm{t}}^2=0.500$ [m^2], and $\mathrm{P}_{\mathrm{FA}}=0.1$. (a) The computed $\mathrm{P}_{\mathrm{CA}}\underline{\mathbb{P}}_{\mathcal{F}}|\mathrm{CA}$ over $N_{\mathrm{sim}}=100$ with $\mu_{\mathrm{sim}}=3.75\cdot10^{-23}$ and $\sigma_{\mathrm{sim}}=1.33\cdot10^{-25}$ and of $\underline{\mathrm{P}}_{\mathrm{FA}}\underline{\mathbb{P}}_{\mathcal{F}}|\mathrm{FA}$ with $\mu_{\mathrm{sim}}=2.57\cdot10^{-12}$ and $\sigma_{\mathrm{sim}}=1.32\cdot10^{-14}$; (b) The μ_{sim} and its σ_{sim} based on $N_{\mathrm{sim}}=100$ of $\mathrm{P}_{\mathrm{MD}_1}\underline{\mathbb{P}}_{\mathcal{F}}|\mathrm{MD}_1$ as a function of b_1; (c) The μ_{sim} and its σ_{sim} based on $N_{\mathrm{sim}}=100$ of $\underline{\mathrm{P}}_{\mathrm{CD}_1}\underline{\mathbb{P}}_{\mathcal{F}}|\mathrm{CD}_1$ as a function of b_1.

while Figures 5(b) and (c) are showing the curves based on the average of the results over $N_{\mathrm{sim}}=100$ (μ_{sim}) and the standard deviation of μ_{sim}'s (denoted σ_{sim}) of $\mathrm{P}_{\mathrm{MD}_1}\underline{\mathbb{P}}_{\mathcal{F}}|\mathrm{MD}_1$ and $\underline{\mathrm{P}}_{\mathrm{CD}_1}\underline{\mathbb{P}}_{\mathcal{F}}|\mathrm{CD}_1$ as a function of the outlier b_1. In Figure 5(a) the large separation between the two components is due to $f_{\underline{\hat{\mathrm{x}}}_1,\underline{\mathrm{t}}}(x,t|\mathcal{H}_0)$ having significantly more probability density over $\mathcal{B}^c\cap\mathcal{P}_1$ than $f_{\underline{\hat{\mathrm{x}}}_0,\underline{\mathrm{t}}}(x,t|\mathcal{H}_0)$ over $\mathcal{B}^c\cap\mathcal{P}_0$ (see Figure 4(a) and (b)). The amount of probability density of $f_{\underline{\hat{\mathrm{x}}}_1,\underline{\mathrm{t}}}(x,t|\mathcal{H}_0)$ over $\mathcal{B}^c\cap\mathcal{P}_1$ is driven by $|\rho_{\underline{\hat{\mathrm{x}}}_1,\underline{\mathrm{t}}}|$, which in this case is 0.7071. To decrease the separation between the two components in Figure 5(a) one would need to decrease $|\rho_{\underline{\hat{\mathrm{x}}}_1,\underline{\mathrm{t}}}|$ (i.e., changing the underlying models in (24)). If $|\rho_{\underline{\hat{\mathrm{x}}}_1,\underline{\mathrm{t}}}|\rightarrow0$, the separation decreases and if $|\rho_{\underline{\hat{\mathrm{x}}}_1,\underline{\mathrm{t}}}|\rightarrow1$, it increases (see Appendix V-B). In this case the MIC of $\underline{\mathbb{P}}_{\mathcal{F}}|\mathcal{H}_0$ is $\underline{\mathrm{P}}_{\mathrm{FA}}\underline{\mathbb{P}}_{\mathcal{F}}|\mathrm{FA}$ and the LIC is $\mathrm{P}_{\mathrm{CA}}\underline{\mathbb{P}}_{\mathcal{F}}|\mathrm{CA}$.

Figure 5(b) displays the behaviour of the result of the integration of $f_{\underline{\hat{\mathrm{x}}}_0,\underline{\mathrm{t}}}(x,t|\mathcal{H}_1)$ over $\mathcal{B}^c\cap\mathcal{P}_0$ as $|\mathrm{b}_1|$ is varied (see Figure 4(c)). Starting from near the value 0, as $|\mathrm{b}_1|\uparrow$ there will be progressively more probability density over $\mathcal{B}^c\cap\mathcal{P}_0$ until a maximum is reached, in this case at $|\mathrm{b}_1|=4.1$ [m] with $\mu_{\mathrm{sim}}=3.37\cdot10^{-10}\pm6.08\cdot10^{-13}$. After this point, the values of μ_{sim} of $\underline{\mathrm{P}}_{\mathrm{MD}_1}\underline{\mathbb{P}}_{\mathcal{F}}|\mathrm{MD}_1$ decreases as $|\mathrm{b}_1|\uparrow$ due to the less probability density over $\mathcal{B}^c\cap\mathcal{P}_0$. The behaviour of σ_{sim} depends on the respective probability density coverage as for a range of $|\mathrm{b}_1|$ it does not cover well both sides of $\mathcal{B}^c$, compared to the case where $|\mathrm{b}_1|$ is larger and it needs to cover only the right-side component of $\mathcal{B}^c$. In Figure 5(c) one can notice the variation of μ_{sim} of $\underline{\mathrm{P}}_{\mathrm{CD}_1}\underline{\mathbb{P}}_{\mathcal{F}}|\mathrm{CD}_1$ in the range of $|\mathrm{b}_1|$ starting from about 2 [m] to about 5 [m], and an almost constant behaviour elsewhere. From the value 0, as $|\mathrm{b}_1|\uparrow$ the probability density of $f_{\underline{\hat{\mathrm{x}}}_1,\underline{\mathrm{t}}}(x,t|\mathcal{H}_1)$ over $\mathcal{B}^c\cap\mathcal{P}_1$ remains almost constant until (approximately) $\approx$ 2 [m] where the probability density over $\mathcal{B}^c\cap\mathcal{P}_0$ starts to be higher, and consequently lower over $\mathcal{B}^c\cap\mathcal{P}_1$. This behaviour is driven by $|\rho_{\hat{\underline{x}}_1,\underline{t}}|$ as for a large correlation there will be a higher probability density over $\mathcal{B}^c \cap \mathcal{P}_0$ in a certain range of $|\mathrm{b}_1|$, while for lower $|\rho_{\hat{\underline{x}}_1,\underline{t}}|$ there will be less probability density. The minimum of $\underline{\mathsf{P}}_{\mathrm{CD}_1}\underline{\mathbb{P}}_{\mathcal{F}}|\mathrm{CD}_1$ is reached at $|\mathrm{b}_1| = 3.6$ [m] where $\mu_{\mathrm{sim}} = 1.31 \cdot 10^{-12} \pm 9.32 \cdot 10^{-15}$, after which the probability density of $f_{\hat{\underline{x}}_1,\underline{t}}(x, t|\mathcal{H}_1)$ over $\mathcal{B}^c \cap \mathcal{P}_1$ increases and stabilizes after $|\mathrm{b}_1| \approx 5$ [m]. The simulation standard deviation σ_{sim} is nearly constant since the respective probability density function consistently covers the four disjoint components of $\mathcal{B}^c \cap \mathcal{P}_1$ regardless of the variation of $|\mathrm{b}_1|$. The MIC of $\underline{\mathbb{P}}_{\mathcal{F}}|\mathcal{H}_1$ for $|\mathrm{b}_1| \in [0,\ 2.5)$[m] and $|\mathrm{b}_1| \in (5.7,\ 7.0]$[m] is $\underline{\mathsf{P}}_{\mathrm{CD}_1}\underline{\mathbb{P}}_{\mathcal{F}}|\mathrm{CD}_1$ (and the LIC $\underline{\mathsf{P}}_{\mathrm{MD}_1}\underline{\mathbb{P}}_{\mathcal{F}}|\mathrm{MD}_1$) while for $|\mathrm{b}_1| \in [2.5,\ 5.7]$[m] the MIC is $\underline{\mathsf{P}}_{\mathrm{MD}_1}\underline{\mathbb{P}}_{\mathcal{F}}|\mathrm{MD}_1$. By summing the μ_{sim}'s from Figure 5 the components $\underline{\mathbb{P}}_{\mathcal{F}}|\mathcal{H}_0$ and $\underline{\mathbb{P}}_{\mathcal{F}}|\mathcal{H}_1(\mathrm{b}_1)$ are obtained (see Figure 6(a) and Figure 6(b)).

If one would have a-priori knowledge about $\mathsf{P}(\mathcal{H}_0)$ or make some assumptions on its values (e.g., $1 - 10^{-3}$, $1 - 10^{-4}$, $1 - 10^{-5}$), then $\underline{\mathbb{P}}_{\mathcal{F}}(\mathrm{b}_1)$ can be computed from its components 'weighted' by these a-priori probabilities. The computed total probability of positioning failure $\underline{\mathbb{P}}_{\mathcal{F}}(\mathrm{b}_1)$ is shown in Figure 6(c) for the three assumptions on $\mathsf{P}(\mathcal{H}_0)$. The behaviour of $\underline{\mathbb{P}}_{\mathcal{F}}(\mathrm{b}_1)$ is driven by $\underline{\mathsf{P}}_{\mathrm{FA}}\underline{\mathbb{P}}_{\mathcal{F}}|\mathrm{FA}$ (the MIC of $\underline{\mathbb{P}}_{\mathcal{F}}|\mathcal{H}_0$) until $|\mathrm{b}_1| \approx 2.2$ [m], after which the μ_{sim} of $\mathsf{P}_{\mathrm{CD}_1}\underline{\mathbb{P}}_{\mathcal{F}}|\mathrm{CD}_1$ takes over until $|\mathrm{b}_1| \approx 2.5$ [m] (MIC of $\underline{\mathbb{P}}_{\mathcal{F}}|\mathcal{H}_1(\mathrm{b}_1)$) and then that of $\mathsf{P}_{\mathrm{MD}_1}\underline{\mathbb{P}}_{\mathcal{F}}|\mathrm{MD}_1$ until $|\mathrm{b}_1| \approx 6.3$ [m] (MIC of $\underline{\mathbb{P}}_{\mathcal{F}}|\mathcal{H}_1(\mathrm{b}_1)$). Past $|\mathrm{b}_1| \approx 6.3$ [m], the influence of $\underline{\mathsf{P}}_{\mathrm{FA}}\underline{\mathbb{P}}_{\mathcal{F}}|\mathrm{FA}$ is again larger. The value of $\underline{\mathbb{P}}_{\mathcal{F}}(\mathrm{b}_1)$ depends on how likely $\mathcal{H}_0$ is considered or assumed to be. If $\mathsf{P}(\mathcal{H}_0) \uparrow$ then the influence of the maximum of the μ_{sim} of $\mathsf{P}_{\mathrm{MD}_1}\underline{\mathbb{P}}_{\mathcal{F}}|\mathrm{MD}_1$ is decreased, while if $\mathsf{P}(\mathcal{H}_0) \downarrow$ its influence increases. If only the maximum value of $\underline{\mathbb{P}}_{\mathcal{F}}(\mathrm{b}_1)$ is of interest, then one can use the results from Table 2.

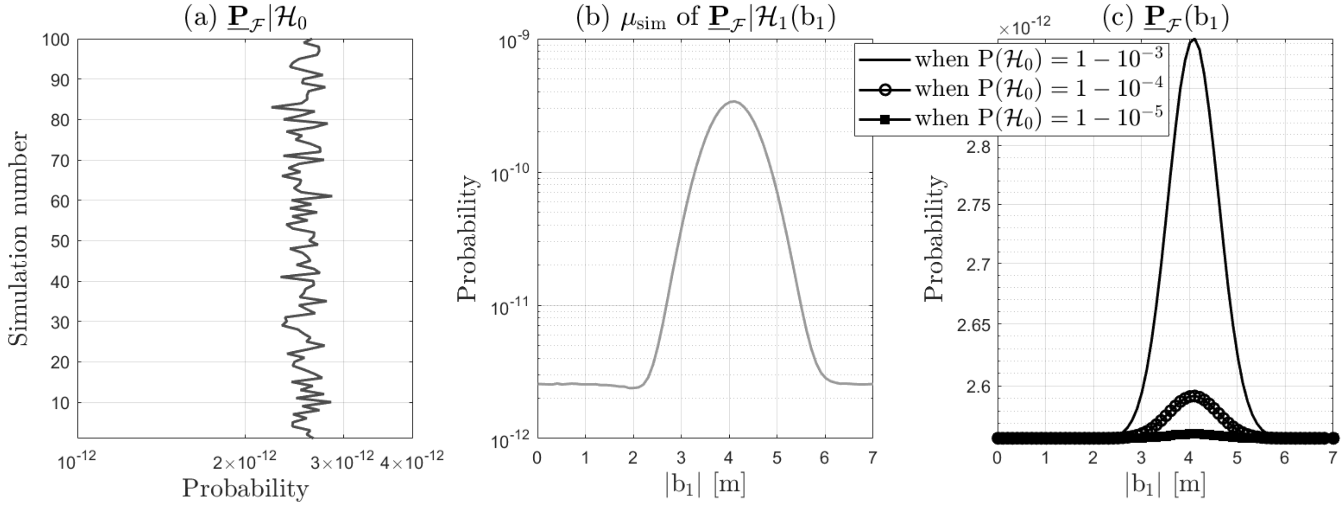

Figure 6: (a); Computed $\underline{\mathbb{P}}_{\mathcal{F}}|\mathcal{H}_0$ over $N_{\mathrm{sim}} = 100$; (b) Computed μ_{sim} of $\underline{\mathbb{P}}_{\mathcal{F}}|\mathcal{H}_1(\mathrm{b}_1)$; (c) Computed total probability of positioning failure $\underline{\mathbb{P}}_{\mathcal{F}}(\mathrm{b}_1)$ for the chosen values for $\mathsf{P}(\mathcal{H}_0)$ ($1 - 10^{-3}$, $1 - 10^{-4}$, and $1 - 10^{-5}$).

Table 2: Maximum values of $\underline{\mathbb{P}}_{\mathcal{F}}(\mathrm{b}_1)$ and their standard deviations (σ_{sim}) from the results in Figure 6(c).

$\mathsf{P}(\mathcal{H}_0)$	Max. $\underline{\mathbb{P}}_{\mathcal{F}}(\mathrm{b}_1)$	σ_{sim}	$\|\mathrm{b}_1\|$ [m]	MIC of $\underline{\mathbb{P}}_{\mathcal{F}}\|\mathcal{H}_0$	MIC of $\underline{\mathbb{P}}_{\mathcal{F}}\|\mathcal{H}_1(\mathrm{b}_1)$ at Max.
$1 - 10^{-3}$	$2.88 \cdot 10^{-12}$	$1.66 \cdot 10^{-14}$	4.1	$\underline{\mathsf{P}}_{\mathrm{FA}}\underline{\mathbb{P}}_{\mathcal{F}}\|\mathrm{FA}$	$\underline{\mathsf{P}}_{\mathrm{MD}_1}\underline{\mathbb{P}}_{\mathcal{F}}\|\mathrm{MD}_1$
$1 - 10^{-4}$	$2.58 \cdot 10^{-12}$	$1.66 \cdot 10^{-14}$	4.1		
$1 - 10^{-5}$	$2.55 \cdot 10^{-12}$	$1.66 \cdot 10^{-14}$	4.1		

At this stage one may ask *"What would be the difference in results by ignoring the dependence between parameter estimation and statistical hypothesis testing?"*. To quantify these differences we can ignore the aforementioned dependence by assuming that the second inequality in (12) becomes an equality: $f^o_{\hat{\underline{x}}_1,\underline{t}}(x, t) = f_{\hat{\underline{x}}_1}(x) f_{\underline{t}}(t)$ (the superscript $[.]^o$ indicates that the dependency is not accounted for). On the basis of this equality the computation of $\underline{\mathbb{P}}^o_{\mathcal{F}}(\mathrm{b}_1)$ can be done to quantify the 'over-optimism' by computing the ratio $\underline{\mathbb{P}}_{\mathcal{F}}(\mathrm{b}_1)/\underline{\mathbb{P}}^o_{\mathcal{F}}(\mathrm{b}_1)$. Figure 7 shows that $\underline{\mathbb{P}}_{\mathcal{F}}(\mathrm{b}_1)/\underline{\mathbb{P}}^o_{\mathcal{F}}(\mathrm{b}_1) > 1$, hence relying on $\underline{\mathbb{P}}^o_{\mathcal{F}}(\mathrm{b}_1)$ can be potentially dangerous. Moreover, $\underline{\mathbb{P}}^o_{\mathcal{F}}(\mathrm{b}_1)$ is around 10 times *lower* than $\underline{\mathbb{P}}_{\mathcal{F}}(\mathrm{b}_1)$ in the intervals where the component under $\mathcal{H}_0$ dominates. The ratio starts to decrease when the component under $\mathcal{H}_1$ starts to drive the behaviour of $\underline{\mathbb{P}}^o_{\mathcal{F}}(\mathrm{b}_1)$ and of $\underline{\mathbb{P}}_{\mathcal{F}}(\mathrm{b}_1)$. At the maximum, $\underline{\mathbb{P}}^o_{\mathcal{F}}(\mathrm{b}_1)$ is : (i) 4.85 times lower than $\underline{\mathbb{P}}_{\mathcal{F}}(\mathrm{b}_1)$ when $\mathsf{P}(\mathcal{H}_0) = 1 - 10^{-3}$; (ii) 8.93 times lower than $\underline{\mathbb{P}}_{\mathcal{F}}(\mathrm{b}_1)$ when $\mathsf{P}(\mathcal{H}_0) = 1 - 10^{-4}$; (iii) 9.86 times lower than $\underline{\mathbb{P}}_{\mathcal{F}}(\mathrm{b}_1)$ when $\mathsf{P}(\mathcal{H}_0) = 1 - 10^{-5}$. Therefore, ignoring the dependence between parameter estimation and statistical hypothesis testing in the above example leads to significantly over-optimistic results.

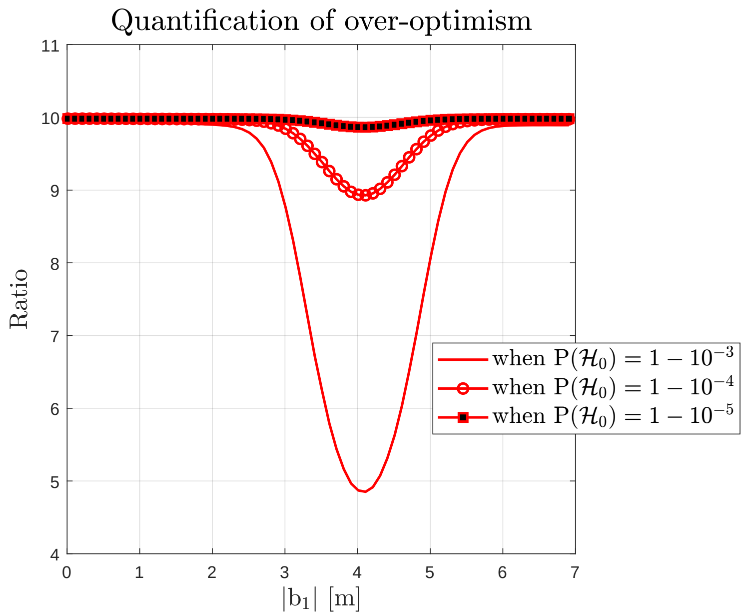

Figure 7: Ratio $\mathbb{P}_{\mathcal{F}}(b_1)/\mathbb{P}^{o}_{\mathcal{F}}(b_1)$ as a function of $|b_1|$ to quantify the over-optimism caused by ignoring the dependence between parameter estimation and statistical hypothesis testing.

2. Differential GNSS-based positioning example

In this GNSS-based positioning safety analysis, we consider a scenario involving an automated vehicle which coordinates are determined in a local East-North-Up (ENU) coordinate system using, single-frequency, code-based pseudorange observables in a Differential GNSS (DGNSS) setup. The GNSS constellations we consider are GPS (G) and Galileo (E), at L1/E1 radio-frequency (1575.42 MHz). Decimeter-level positioning precision for the rover receiver (installed in the automated vehicle) can be achieved, depending on the distance between the reference station and the rover receiver (Kealy and Moore, 2017). The (linearized) DGNSS positioning model is (Odijk, 2017)

$$\mathsf{E}_{f_{\underline{y}}}\underbrace{\left(\begin{bmatrix}\underline{y}_{G}\\ \underline{y}_{E}\end{bmatrix}\right)}_{\underline{y}}=\underbrace{\begin{bmatrix}U_{G} & \mathbf{u}_{G}\\ U_{E} & \mathbf{u}_{E}\end{bmatrix}}_{A}\underbrace{\begin{bmatrix}\Delta\mathbf{p}\\ \mathsf{c}\,\Delta\mathbf{t}\end{bmatrix}}_{\Delta x},\quad Q_{yy}=\mathrm{blkdiag}[Q_{y_{G}y_{G}},Q_{y_{E}y_{E}}]\text{ with }\underline{y}\sim\mathcal{N}\left(A\Delta x,Q_{yy}\right). \tag{33}$$

In (33), the entries of $\underline{y}_{[.]} \in \mathbb{R}^{m_{[.]}}$, where $[.] \in \{\text{G or E}\}$, represent the observed pseudoranges from which the Euclidean distances between a chosen linearization point and the satellites are subtracted, and the pseudorange corrections are applied by addition. The application of the pseudorange corrections remove most of the satellite orbit errors and remove the satellite clock error and satellite code hardware bias. For distances between the reference and rover receiver up to 10 km, the differential delays due to the troposphere and ionosphere can be considered negligible (Odijk, 2002). The DGNSS positioning model in (33) considers that both the reference and rover receivers have calibrated the GPS-Galileo Inter System Bias by applying it as an additional correction to their pseudoranges (Odijk, 2017). The matrix $U_{[.]} \in \mathbb{R}^{m_{[.]}\times 3}$ contains the unit direction vectors between the rover receiver and the satellites (with the minus sign from the linerization accounted for), and $\mathbf{u}_{[.]} = [1 \quad 1 \quad \dots \quad 1]^T \in \mathbb{R}^{m_{[.]}}$. The unknown parameters are the rover's ENU coordinate increments $\Delta\mathbf{p} \in \mathbb{R}^3$ and $\Delta\mathbf{t} \in \mathbb{R}$ which represents the combined differential receiver clock and hardware delay. The c term is the speed of light in a vacuum. The design matrix $A \in \mathbb{R}^{m\times n}$ has $\mathrm{rank}(A) = n = 4$, where $m = m_G + m_E$. The variance-covariance matrix $Q_{y_{[.]}y_{[.]}} = 2\sigma^2_{y_{[.]}} W^{-1}_{[.]} \in \mathbb{R}^{m_{[.]}\times m_{[.]}}$ is diagonal with $W_{[.]} = \mathrm{diag}[\omega_{1_{[.]}}, \dots, \omega_{m_{[.]}}] \in \mathbb{R}^{m_{[.]}\times m_{[.]}}$ being the weight matrix which components are the elevation-dependent weighting functions as given in (Euler and Goad, 1991). In $Q_{y_{[.]}y_{[.]}}$, $\sigma_{y_{[.]}}$ is the standard deviation of the pseudorange observables, in [m], and the factor 2 is due to the application of the pseudorange corrections to the observed pseudoranges by the rover receiver (assuming the same $\sigma_{y_{[.]}}$ at both reference and rover receivers (Hauschild, 2017)). For the analysis in this section, we aim for a horizontal positioning precision of about 0.5 meters (95% circular probability radius). To achieve this, we set $\sqrt{2}\sigma_{y_G} = 0.3$ [m] and $\sqrt{2}\sigma_{y_E} = 0.2$ [m], which correspond to achievable positioning precisions based on DGNSS (Kealy and Moore, 2017).

The redundancy of the model in (33) is $r = m - \mathrm{rank}(A) = (m_G + m_E) - 4$. The estimate $\hat{x}$ is obtained from a Gauss-Newton iteration scheme once the stop criterion is met for $\Delta\hat{x}$ (Teunissen, 1990). We account for individual outliers in the observations and assume that only one observation outlier occurs at a time. This is the case of datasnooping (Baarda, 1968) with

$$\mathcal{H}_0 : \mathsf{E}_{f_{\underline{y}}}\left(\underline{y}\right) = A\,\Delta x \quad \text{vs.} \quad \mathcal{H}_i : \mathsf{E}_{f_{\underline{y}}}\left(\underline{y}\right) = A\,\Delta x + c_i b_i \text{ for } i \in \{1, ..., k\}, \tag{34}$$

where $k = m$, $c_i = \begin{cases} 0_m, & \text{if } i = 0 \\ [0 \;\dots\; 0 \;\dots\; 1 \;\dots\; 0]^T \in \mathbb{R}^m, & \text{if } i > 0 \end{cases}$ is the canonical unit vector, $b_i \in \mathbb{R}$ is the unknown outlier with its size in meters, and $\text{rank}([A, c_i]) = 5$. The resulting partitions of $\mathbb{R}^r$, given a level of significance $\alpha = \mathsf{P}_{\text{FA}}$, are

$$\mathcal{P}_0 = \left\{t \in \mathbb{R}^r \mid ||t||^2_{Q_{tt}} \leq \chi^2_\alpha(r, 0)\right\}, \quad \mathcal{P}_i = \left\{t \in \mathbb{R}^r \mid t \notin \mathcal{P}_0,\ |w_i| = \max_{j\in\{1,\dots,k\}} |w_j|\right\} \text{ for } i \in \{1, ..., k\}, \tag{35}$$

where $|\underline{w}_j| = ||\mathbf{Q}_{c_{t_j}} \underline{t}||_{Q_{tt}}$ is the w-test statistic (Baarda, 1967; Teunissen, 2024b). The skyplot in Figure 8(a) shows the positions of the GNSS satellites, as observed by the rover receiver. The satellite geometry consists of $m_G = 8$ GPS satellites (blue) and $m_E = 7$ Galileo satellites (orange) with an elevation cut-off angle of $10°$.

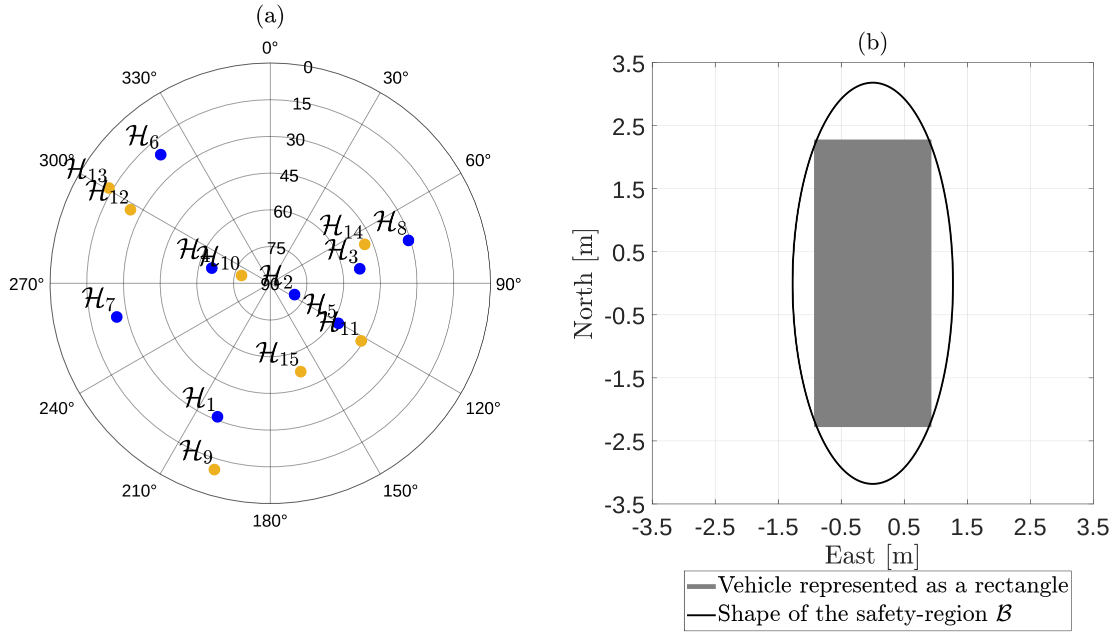

Figure 8: (a) Skyplot view of the rover receiver (vehicle)-satellite geometry. The blue dots are representing the GPS satellites, while the orange ones represents the Galileo satellites and the corresponding $\mathcal{H}_i$'s, for $i \in \{1, ..., 15\}$; (b) Shape that bounds the vehicle and the shape of the safety-region $\mathcal{B} \subset \mathbb{R}^2$.

In this setup, the misclosure vector $\underline{t} = B^T\underline{y}$ belongs to $\mathbb{R}^{r=11}$. We focus the analysis on the 2D position of the vehicle as the horizontal domain is most relevant: $\underline{\bar{h}} = H^T\underline{\bar{x}}$ where $H^T = [I_2 \quad 0_{2\times2}]$ and $\underline{\bar{x}} = \underline{\hat{x}}_0 - \sum_{i=1}^k L_i\, \underline{t}\, p_i(\underline{t})$ is the n-dimensional DIA-estimator. The PDF of $\underline{\bar{h}}$ is

$$f_{\underline{\bar{h}}}(h) = f_{\underline{\hat{h}}_0}(h) \int_{\mathcal{P}_0} f_{\underline{t}}(t)dt + \sum_{i=1}^{k=15} \int_{\mathcal{P}_i} f_{\underline{\hat{h}}_0}\left(h + H^T L_i\, t\right) f_{\underline{t}}(t)dt, \tag{36}$$

with $f_{\underline{\hat{h}}_0}(h) \overset{\mathcal{H}_0}{=} \mathcal{N}\left(h,\ Q_{\hat{h}_0\hat{h}_0} = H^T Q_{\hat{x}_0\hat{x}_0} H\right)$ and $f_{\underline{t}}(t) \overset{\mathcal{H}_0}{=} \mathcal{N}\left(0_r,\ Q_{tt} = B^T Q_{yy} B\right)$. When determining the shape and size of the safety-region $\mathcal{B} \subset \mathbb{R}^2$, several factors should be considered, such as: (i) vehicle's dimensions, (ii) road geometry to ensure that all the elements $h \in \mathbb{R}^2$ inside the set $\mathcal{B} \subset \mathbb{R}^2$ are such that the vehicle is within its lane, (iii) minimum required braking distance as a function of the vehicle's speed, (iv) proximity w.r.t. other traffic participants, among other considerations. Several approaches have been proposed in terms of shapes of the safety-region that bound the vehicle (e.g., elliptical, rectangular) in several studies (Kigotho and Rife, 2021; Reid et al., 2019; Feng et al., 2018). As an example, and for consistency with existing approaches in the literature, we choose an ellipse to inscribe the vehicle which has a length of 4.5 [m], a width of 1.8 [m], and an orientation of 0° relative to the vertical axis. For a single-epoch in time, the safety-region is defined as

$$\mathcal{B} = \{h \in \mathbb{R}^2 \mid ||h - \mathrm{h}_{\mathrm{true}}||^2_{\mathrm{Q}_{\mathcal{B}}} \leq 1\}, \tag{37}$$

where $\mathrm{Q}_{\mathcal{B}}^{-1} = \begin{bmatrix} 0.6173 & 0 \\ 0 & 0.0988 \end{bmatrix}$ $[\mathrm{m}^{-2}]$ and $\mathrm{h}_{\mathrm{true}} \in \mathbb{R}^2$ is the true location of the vehicle (set at 0_2 for this example). The safety-region $\mathcal{B} \in \mathbb{R}^2$, which inscribes the vehicle, has a major axis length of 6.36 [m] and a minor axis length of 2.55 [m] (Figure 8(b)). In the following two subsections we discuss the resulting PDFs and probabilities of positioning failure.

a) Probability density functions of $\underline{\bar{\mathrm{h}}} \in \mathbb{R}^2$ under $\mathcal{H}_0$ and a $\mathcal{H}_{i\neq 0}$

The components of $f_{\underline{\bar{\mathrm{h}}}}(h|\mathcal{H}_0)$ are displayed in Figure 9. Under the event of CA, the precision of the horizontal position components is $\sigma_{\hat{\mathrm{h}}_0,\mathrm{east}} = 0.17$ [m], $\sigma_{\hat{\mathrm{h}}_0,\mathrm{north}} = 0.23$ [m], and the correlation coefficient is $\rho_{\hat{\mathrm{h}}_0} = 0.16$.

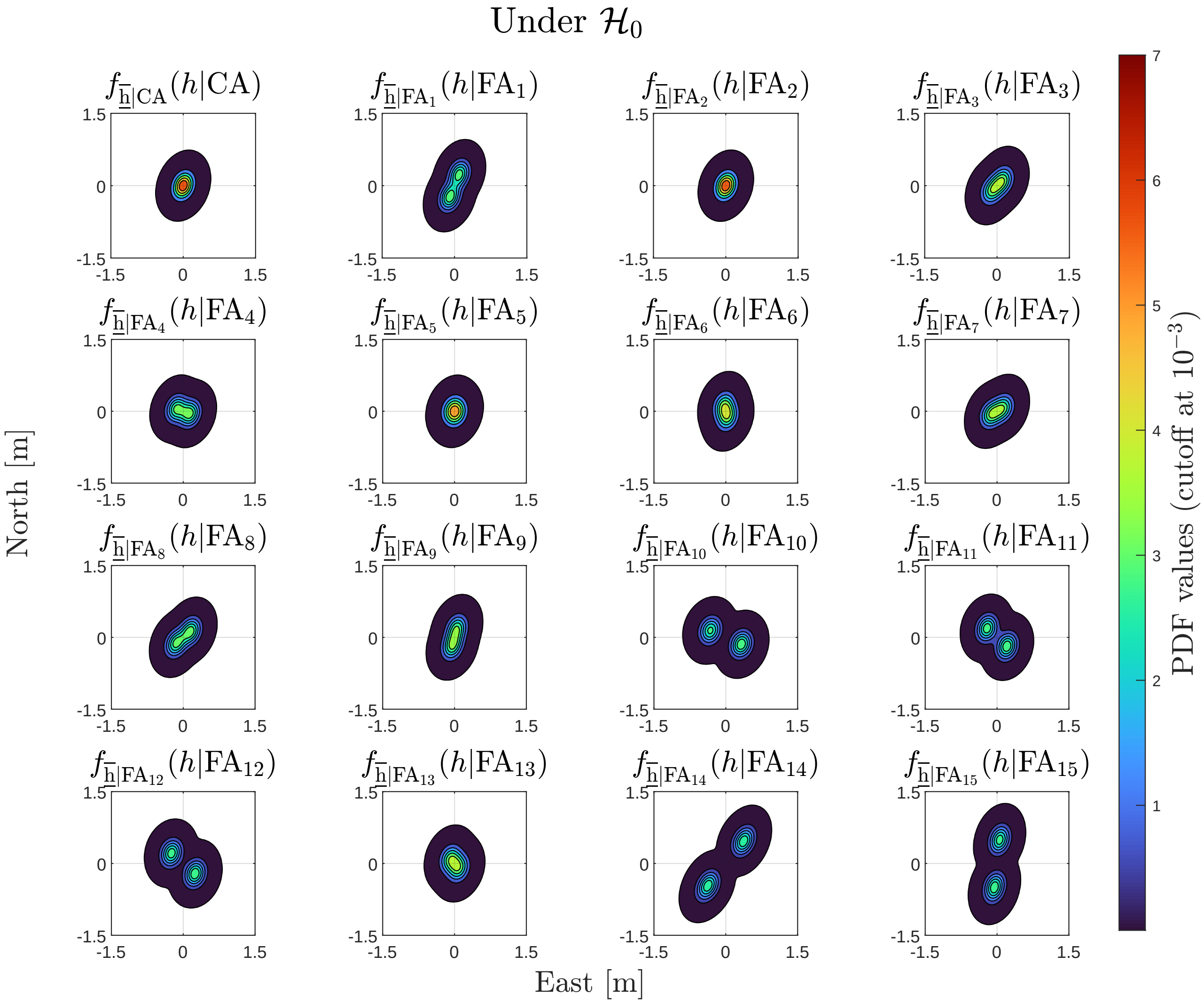

Figure 9: Components of $f_{\underline{\bar{\mathrm{h}}}}(h|\mathcal{H}_0)$ for $\mathrm{P}_{\mathrm{FA}} = 10^{-3}$.

The properties of $f_{\underline{\bar{\mathrm{h}}}|\mathrm{FA}_i}(h|\mathrm{FA}_i)$ (e.g., orientation, multimodality) are driven by the averaged shifted functions $f_{\underline{\hat{\mathrm{h}}}_0}\left(h + \mathrm{H}^T\mathrm{L}_i\, t|\mathcal{H}_0\right)$. Examining $\mathrm{H}^T\mathrm{L}_i\, \underline{\mathrm{t}}$ will provide insights about the properties of $f_{\underline{\bar{\mathrm{h}}}|\mathrm{FA}_i}(h|\mathrm{FA}_i)$. If we express

$$\mathrm{H}^T\mathrm{L}_i\, \underline{\mathrm{t}} = \mathrm{H}^T\mathrm{A}^+\mathrm{c}_i\mathrm{c}_{\mathrm{t}_i}^+\, \underline{\mathrm{t}} = \mathrm{H}^T\mathrm{Q}_{\hat{\mathrm{x}}_0\hat{\mathrm{x}}_0}\mathrm{A}^T\mathrm{Q}_{\mathrm{yy}}^{-1}\mathrm{c}_i\,(\mathrm{c}_{\mathrm{t}_i}^+\,\underline{\mathrm{t}}) = \mathrm{g}_i\,(\mathrm{c}_{\mathrm{t}_i}^+\,\underline{\mathrm{t}}) \text{ for } i \in \{1, ..., k\}, \tag{38}$$

where $g_i \in \mathbb{R}^2$ and $(c_{t_i}^{+}\underline{t}) \in \mathbb{R}$. The angle of $\mathcal{R}(g_i)$ w.r.t. the horizontal axis is driven by the design matrix A and by $Q_{y_{[.]}y_{[.]}}$ through $Q_{\hat{x}_0\hat{x}_0}$. The rows of $(H^T Q_{\hat{x}_0\hat{x}_0}) \in \mathbb{R}^{2\times n}$ (variances of the components on East and North directions, the covariance between them, and their covariances with the Up component and $\Delta\mathbf{t}$) are influencing the orientation of $\mathcal{R}(g_i)$ by transforming the scaled rows of A obtained from $(A^T Q_{yy}^{-1} c_i) \in \mathbb{R}^n$. As a result, $\mathcal{R}(g_i)$ drives the orientation of $f_{\underline{\bar{h}}|FA_i}(h|FA_i)$. The multimodality is driven by how the term $(c_{t_i}^{+}\underline{t})$ varies across $\mathcal{R}(g_i)$ for $\underline{t} \in \mathcal{P}_i$. One can relate the shape of the safety-region $\mathcal{B}$ from Figure 8(b) with the components of $f_{\underline{\bar{h}}}(h|\mathcal{H}_0)$ in Figure 9 to identify which ones have a large or small probability density outside $\mathcal{B}$. For example, the components $f_{\underline{\bar{h}}|FA_{10}}(h|FA_{10})$, $f_{\underline{\bar{h}}|FA_{12}}(h|FA_{12})$, and $f_{\underline{\bar{h}}|FA_{14}}(h|FA_{14})$ are oriented transversely with respect to $\mathcal{B}$ and have their mode the furthest apart. This indicates that these components have the largest probability density outside of $\mathcal{B}$ when compared with the other components.

The PDF of $\underline{\bar{h}} \in \mathbb{R}^2$ under any $\mathcal{H}_{i\neq 0}$ depends on the size of the outlier b_i. For this reason one needs to choose or make assumptions on the size of b_i. As an example, we show the components of $f_{\underline{\bar{h}}}(h|\mathcal{H}_{10})$ for $b_{10} = 1$ [m] in Figure 10. When $b_{10} \neq 0$ there is no symmetry of $f_{\underline{t}}(t|\mathcal{H}_{10})$ w.r.t. the origin of $\mathbb{R}^r$ and w.r.t. the partitions $\mathcal{P}_i$. The shape and modes of the conditional components is driven by the outcome of the averaged shifted functions $f_{\underline{\hat{h}}_0}\left(h + H^T L_i\, t|\mathcal{H}_{14}\right)$ for $\underline{t} \in \mathcal{P}_i$ with $\underline{t} \overset{\mathcal{H}_{10}}{\sim} \mathcal{N}\left(c_{t_{10}} b_{10},\ Q_{tt} = B^T Q_{yy} B\right)$ and $i \in \{0, ..., k\}$ (see (36)).

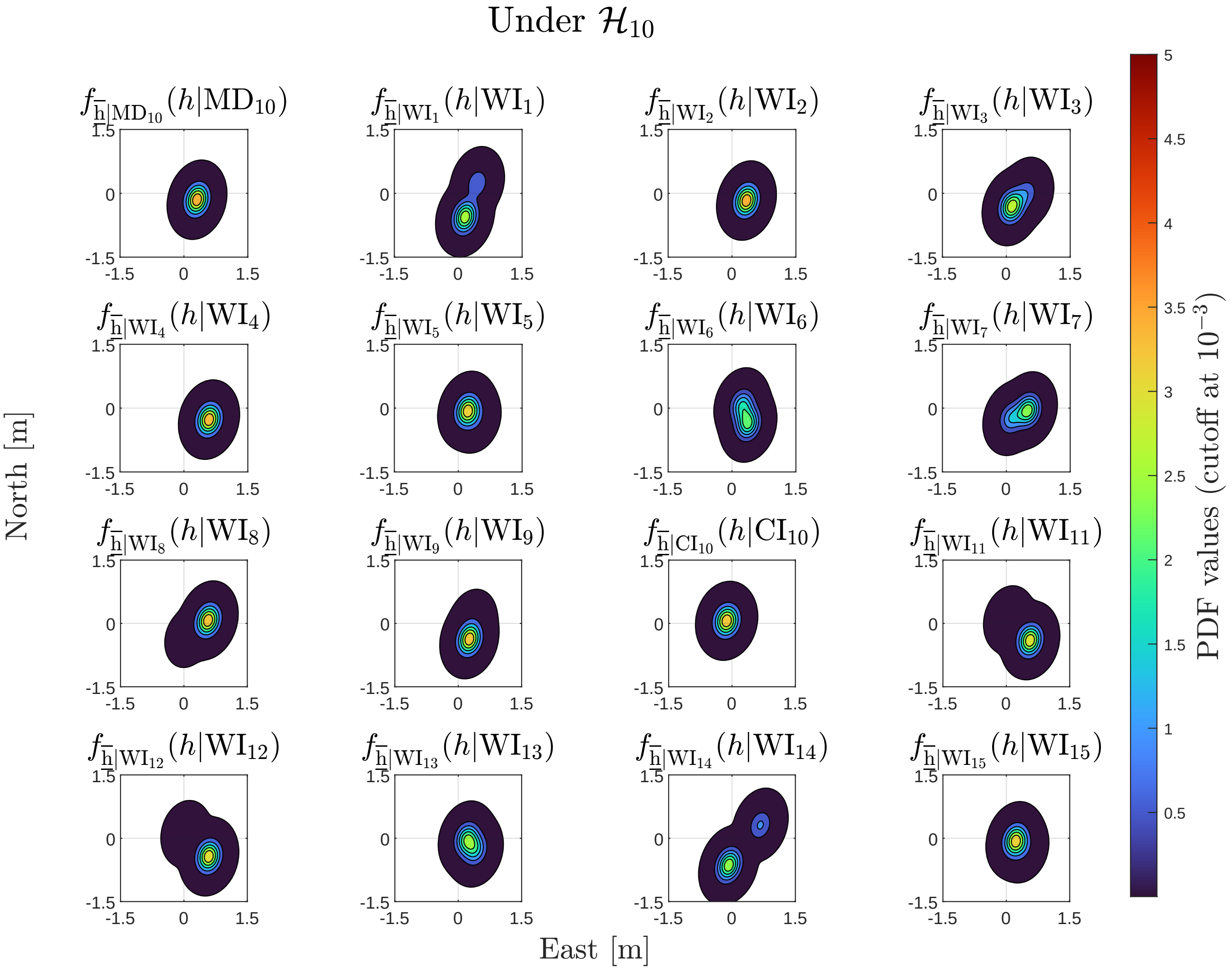

Figure 10: Components of $f_{\underline{\bar{h}}}(h|\mathcal{H}_{10})$ for $b_{10} = 1$ [m] and $P_{FA} = 10^{-3}$.

b) Probability of positioning failure for a fixed safety-region $\mathcal{B} \subset \mathbb{R}^2$

The next step is to compute $\mathbb{P}_{\mathcal{F}}|\mathcal{H}_0 = \sum_{j=0}^{k=15} \mathsf{E}_{f_{\underline{\hat{x}}_j,\underline{t}}}\left(\mathbb{1}_j(\underline{x},\underline{t})|\mathcal{H}_0\right)$ and $\mathbb{P}_{\mathcal{F}}|\mathcal{H}_{10}(\mathrm{b}_{10}) = \sum_{j=0}^{k=15} \mathsf{E}_{f_{\underline{\hat{x}}_j,\underline{t}}}\left(\mathbb{1}_j(\underline{x},\underline{t})|\mathcal{H}_{10}\right)$ (see (21)) using the safety-region $\mathcal{B} \subset \mathbb{R}^2$ defined in (37). A similar route is followed for the components under the other $\mathcal{H}_{i\neq 0}$'s. The components of the computed $\underline{\mathbb{P}}_{\mathcal{F}}|\mathcal{H}_0$ are displayed in Table 3 and those of $\underline{\mathbb{P}}_{\mathcal{F}}|\mathcal{H}_{10}(\mathrm{b}_{10})$ in Figure 11.

Table 3: Components of $\underline{\mathbb{P}}_{\mathcal{F}}|\mathcal{H}_0$ for $\mathsf{P}_{\mathrm{FA}} = 10^{-3}$. The results are obtained over $N_{\mathrm{sim}} = 50$ based on which the mean values (μ_{sim}) and the standard deviations of the mean values (σ_{sim}) were computed.

Component of $\underline{\mathbb{P}}_{\mathcal{F}}\|\mathcal{H}_0$	μ_{sim}	σ_{sim} of μ_{sim}
$\mathsf{P}_{\mathrm{CA}}\underline{\mathbb{P}}_{\mathcal{F}}\|\mathrm{CA}$	$2.29 \cdot 10^{-13}$	$7.19 \cdot 10^{-16}$
$\underline{\mathsf{P}}_{\mathrm{FA}_1}\underline{\mathbb{P}}_{\mathcal{F}}\|\mathrm{FA}_1$	$1.18 \cdot 10^{-14}$	$4.04 \cdot 10^{-16}$
$\underline{\mathsf{P}}_{\mathrm{FA}_2}\underline{\mathbb{P}}_{\mathcal{F}}\|\mathrm{FA}_2$	$2.71 \cdot 10^{-17}$	$1.41 \cdot 10^{-18}$
$\underline{\mathsf{P}}_{\mathrm{FA}_3}\underline{\mathbb{P}}_{\mathcal{F}}\|\mathrm{FA}_3$	$1.86 \cdot 10^{-14}$	$4.66 \cdot 10^{-16}$
$\underline{\mathsf{P}}_{\mathrm{FA}_4}\underline{\mathbb{P}}_{\mathcal{F}}\|\mathrm{FA}_4$	$1.22 \cdot 10^{-13}$	$2.01 \cdot 10^{-15}$
$\underline{\mathsf{P}}_{\mathrm{FA}_5}\underline{\mathbb{P}}_{\mathcal{F}}\|\mathrm{FA}_5$	$3.30 \cdot 10^{-16}$	$1.06 \cdot 10^{-17}$
$\underline{\mathsf{P}}_{\mathrm{FA}_6}\underline{\mathbb{P}}_{\mathcal{F}}\|\mathrm{FA}_6$	$1.19 \cdot 10^{-16}$	$4.21 \cdot 10^{-18}$
$\underline{\mathsf{P}}_{\mathrm{FA}_7}\underline{\mathbb{P}}_{\mathcal{F}}\|\mathrm{FA}_7$	$4.40 \cdot 10^{-14}$	$7.92 \cdot 10^{-16}$
$\underline{\mathsf{P}}_{\mathrm{FA}_8}\underline{\mathbb{P}}_{\mathcal{F}}\|\mathrm{FA}_8$	$3.46 \cdot 10^{-13}$	$6.05 \cdot 10^{-15}$
$\underline{\mathsf{P}}_{\mathrm{FA}_9}\underline{\mathbb{P}}_{\mathcal{F}}\|\mathrm{FA}_9$	$8.34 \cdot 10^{-17}$	$4.55 \cdot 10^{-18}$
$\underline{\mathsf{P}}_{\mathrm{FA}_{10}}\underline{\mathbb{P}}_{\mathcal{F}}\|\mathrm{FA}_{10}$	$4.32 \cdot 10^{-12}$	$4.82 \cdot 10^{-14}$
$\underline{\mathsf{P}}_{\mathrm{FA}_{11}}\underline{\mathbb{P}}_{\mathcal{F}}\|\mathrm{FA}_{11}$	$1.84 \cdot 10^{-13}$	$3.06 \cdot 10^{-15}$
$\underline{\mathsf{P}}_{\mathrm{FA}_{12}}\underline{\mathbb{P}}_{\mathcal{F}}\|\mathrm{FA}_{12}$	$4.96 \cdot 10^{-13}$	$7.34 \cdot 10^{-15}$
$\underline{\mathsf{P}}_{\mathrm{FA}_{13}}\underline{\mathbb{P}}_{\mathcal{F}}\|\mathrm{FA}_{13}$	$4.37 \cdot 10^{-16}$	$1.82 \cdot 10^{-17}$
$\underline{\mathsf{P}}_{\mathrm{FA}_{14}}\underline{\mathbb{P}}_{\mathcal{F}}\|\mathrm{FA}_{14}$	$8.92 \cdot 10^{-11}$	$8.41 \cdot 10^{-13}$
$\underline{\mathsf{P}}_{\mathrm{FA}_{15}}\underline{\mathbb{P}}_{\mathcal{F}}\|\mathrm{FA}_{15}$	$3.53 \cdot 10^{-16}$	$1.48 \cdot 10^{-17}$
$\underline{\mathbb{P}}_{\mathcal{F}}\|\mathcal{H}_0$	$9.50 \cdot 10^{-11}$	$8.42 \cdot 10^{-13}$

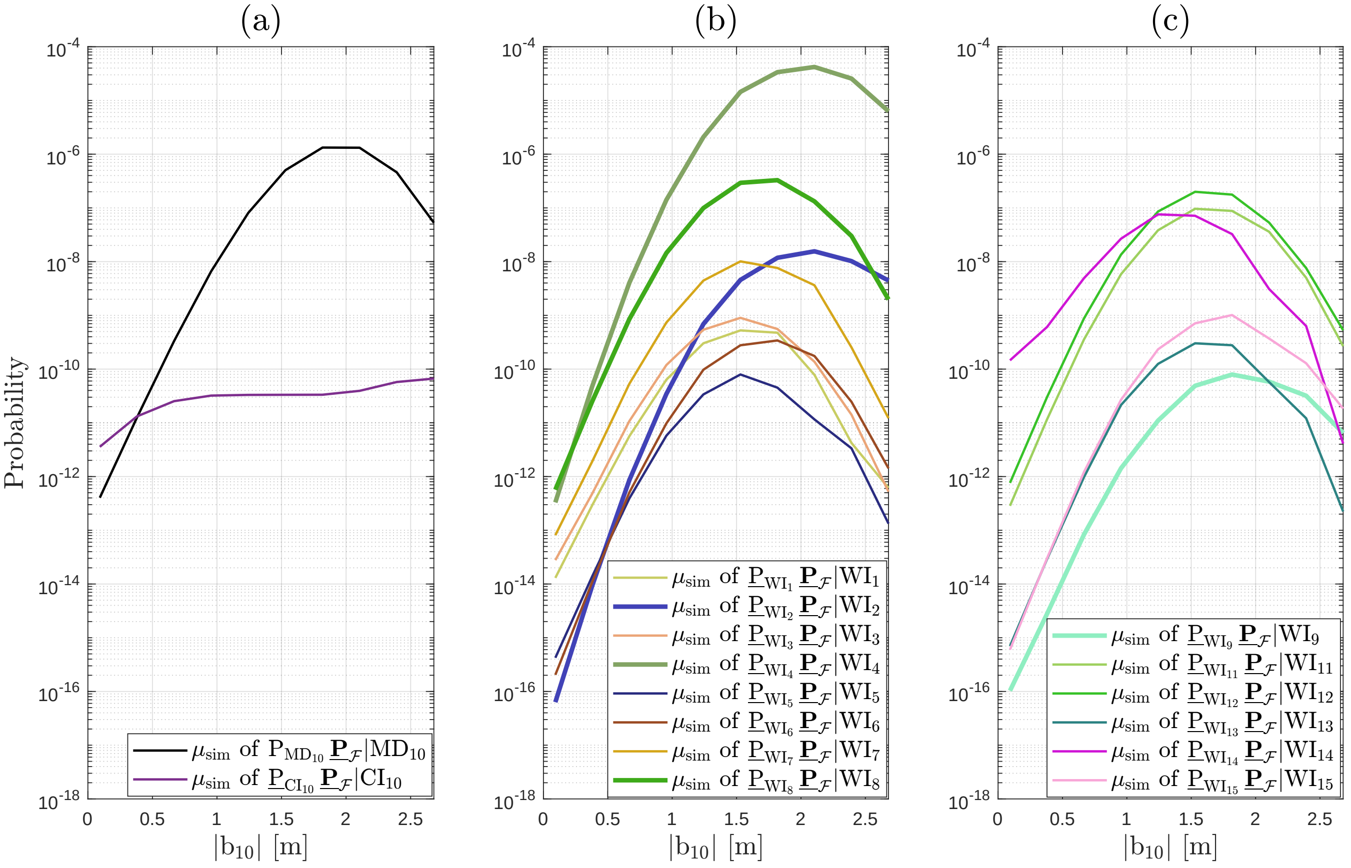

Figure 11: Components of $\underline{\mathbb{P}}_{\mathcal{F}}|\mathcal{H}_{10}(\mathrm{b}_{10})$ for range of outliers $|\mathrm{b}_{10}|$, and $\mathsf{P}_{\mathrm{FA}} = 10^{-3}$. Curves are mean values (μ_{sim}) obtained based on $N_{\mathrm{sim}} = 50$. Mean values of components are: (a) under MD_{10} and CI_{10}; (b) under WI_j corresponding to GPS satellites (for $j \in \{1, ..., 8\}$); (c) under WI_j corresponding to Galileo satellites (for $j \in \{9, 11, ..., 15\}$)

From Table 3 we observe that the MIC of $\underline{\mathbb{P}}_{\mathcal{F}}|\mathcal{H}_0$ is $\underline{\mathsf{P}}_{\mathrm{FA}_{14}}\underline{\mathbb{P}}_{\mathcal{F}}|\mathrm{FA}_{14}$ with $\mu_{\text{sim}} = 8.92 \cdot 10^{-11} \pm 8.41 \cdot 10^{-13}$. This result is due to the two modes of $f_{\overline{\underline{\mathrm{h}}}|\mathrm{FA}_{14}}(h|\mathrm{FA}_{14})$ being most distant from each other along the principal axis (see Figure 9), which is also approximately diagonal to the safety-region $\mathcal{B}$. Conversely, $f_{\overline{\underline{\mathrm{h}}}|\mathrm{FA}_2}(h|\mathrm{FA}_2)$ (corresponds to the highest elevation satellite) does not show multimodality or elongations which leads to the LIC of $\underline{\mathbb{P}}_{\mathcal{F}}|\mathcal{H}_0$ to be $\underline{\mathsf{P}}_{\mathrm{FA}_2}\underline{\mathbb{P}}_{\mathcal{F}}|\mathrm{FA}_2$ with $\mu_{\text{sim}} = 2.71 \cdot 10^{-17} \pm 1.41 \cdot 10^{-18}$.

Regarding the components of $\underline{\mathbb{P}}_{\mathcal{F}}|\mathcal{H}_{10}(\mathrm{b}_{10})$, Figure 11(a) shows the ones under MD_{10} and CI_{10} where the maximum of the μ_{sim} of the former is reached at $1.33 \cdot 10^{-6} \pm 7.74 \cdot 10^{-9}$ for $|\mathrm{b}_{14}| = 1.82$ [m] and that of the latter at $6.65 \cdot 10^{-11} \pm 2.97 \cdot 10^{-12}$ for $|\mathrm{b}_{10}| = 2.68$ [m]. As the outlier $|\mathrm{b}_{10}| \rightarrow \infty$, the probability density of $f_{\overline{\underline{\mathrm{h}}}|\mathrm{MD}_{10}}(h|\mathrm{MD}_{10})$ increases in $\mathcal{B}^c$, while $\mathsf{P}_{\mathrm{MD}_{10}}$ goes to 0, and the latter will drive the entire component $\mathsf{P}_{\mathrm{MD}_{10}}\underline{\mathbb{P}}_{\mathcal{F}}|\mathrm{MD}_{10}$ towards 0. After $\mathsf{P}_{\mathrm{MD}_{10}}\underline{\mathbb{P}}_{\mathcal{F}}|\mathrm{MD}_{10}$ reaches its maximum, the decrease is driven by $\mathsf{P}_{\mathrm{MD}_{10}}$ as its value is significantly smaller than that of $\underline{\mathbb{P}}_{\mathcal{F}}|\mathrm{MD}_{10}$. From Figures 11(b) and 11(c) we observe that the component under WI_{14} is the MIC of $\underline{\mathbb{P}}_{\mathcal{F}}|\mathcal{H}_{10}(\mathrm{b}_{10})$ for $|\mathrm{b}_{10}| < 0.70$ [m] while for $|\mathrm{b}_{10}| > 0.70$ [m] the MIC is the component under WI_4. The value of the μ_{sim} of $\underline{\mathsf{P}}_{\mathrm{WI}_4}\underline{\mathbb{P}}_{\mathcal{F}}|\mathrm{WI}_4$ at the maximum is $4.20 \cdot 10^{-5} \pm 2.86 \cdot 10^{-6}$ for $|\mathrm{b}_{10}| = 2.10$ [m]. A similar type of analysis applies for the LICs as a function of $|\mathrm{b}_{10}|$ (e.g., μ_{sim} of $\underline{\mathsf{P}}_{\mathrm{WI}_2}\underline{\mathbb{P}}_{\mathcal{F}}|\mathrm{WI}_2$, μ_{sim} of $\underline{\mathsf{P}}_{\mathrm{WI}_5}\underline{\mathbb{P}}_{\mathcal{F}}|\mathrm{WI}_5$, μ_{sim} of $\underline{\mathsf{P}}_{\mathrm{WI}_9}\underline{\mathbb{P}}_{\mathcal{F}}|\mathrm{WI}_9$).

On the basis of the previous step we compute the probabilities of positioning failure under $\mathcal{H}_0$ and under each alternative hypothesis $\mathcal{H}_{i\neq 0}$ by summing the corresponding μ_{sim}'s (e.g., ones from Figure 11 for $\mathcal{H}_0$ and $\mathcal{H}_{10}$), and show the results in Figure 12. It is noticeable that $\underline{\mathbb{P}}_{\mathcal{F}}|\mathcal{H}_4(\mathrm{b}_4)$, $\underline{\mathbb{P}}_{\mathcal{F}}|\mathcal{H}_8(\mathrm{b}_8)$, $\underline{\mathbb{P}}_{\mathcal{F}}|\mathcal{H}_{10}(\mathrm{b}_{10})$, and $\underline{\mathbb{P}}_{\mathcal{F}}|\mathcal{H}_{14}(\mathrm{b}_{14})$ are dominating when $|\mathrm{b}_i| > 1.60$ [m].

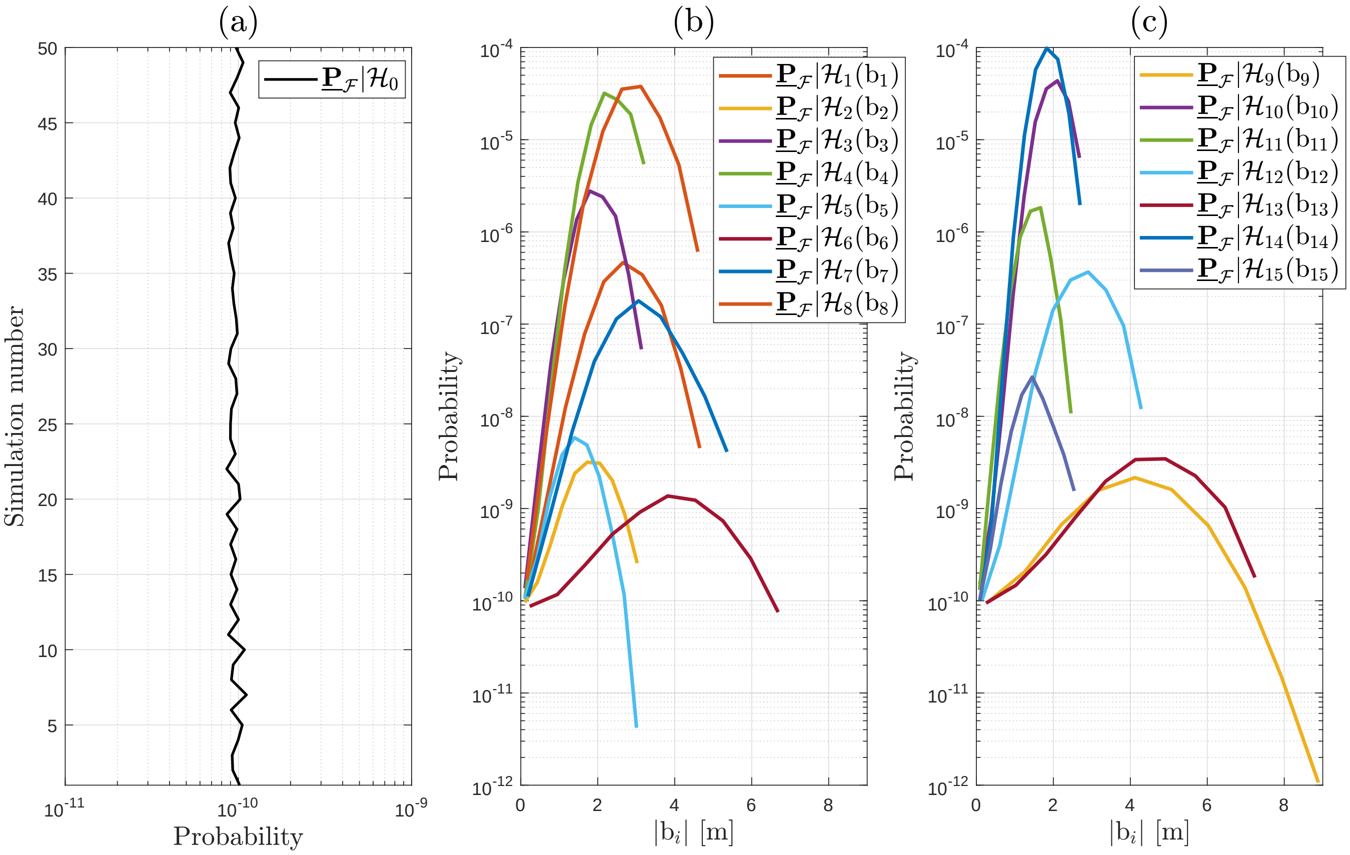

Figure 12: Probabilities of positioning failure under $\mathcal{H}_0$ and under each alternative hypothesis $\mathcal{H}_{i\neq 0}$ for ranges of outliers. (a) $\underline{\mathbb{P}}_{\mathcal{F}}|\mathcal{H}_0$ over $N_{\text{sim}} = 50$; (b) $\underline{\mathbb{P}}_{\mathcal{F}}|\mathcal{H}_i(\mathrm{b}_i)$ corresponding to GPS satellites (for $i \in \{1, ..., 8\}$); (c) $\underline{\mathbb{P}}_{\mathcal{F}}|\mathcal{H}_i(\mathrm{b}_i)$ corresponding to Galileo satellites (for $i \in \{9, 11, ..., 15\}$)

Based on the receiver-satellite geometry (Figure 8(a)) and the elevation-based weighting, satellites 4, 8, 10, and 14 have a large influence on the horizontal-axis (east-component) of the 2D position solution. Relating this aspect to the shape of the safety-region $\mathcal{B}$ from Figure 8(b), variations across the East-component of the PDFs $f_{\overline{\underline{\mathrm{h}}}}(h|\mathcal{H}_4)$, $f_{\overline{\underline{\mathrm{h}}}}(h|\mathcal{H}_8)$, $f_{\overline{\underline{\mathrm{h}}}}(h|\mathcal{H}_{10})$, and $f_{\overline{\underline{\mathrm{h}}}}(h|\mathcal{H}_{14})$ are driving the respective probabilities of positioning failure. Satellites at low-elevations have a reduced contribution to the 2D position solution (e.g., 6, 9, and 13) which leads to low probabilities of positioning failure under the respective alternative hypotheses. The computed $\underline{\mathbb{P}}_{\mathcal{F}}|\mathcal{H}_0$ and the maximum of each $\underline{\mathbb{P}}_{\mathcal{F}}|\mathcal{H}_{i\neq 0}(\mathrm{b}_i)$ are shown in Table 6 of Appendix V-C. We also present the results in Table 7 of Appendix V-C for the case where the dependence between parameter estimation and statistical hypothesis testing is ignored when computing $\underline{\mathbb{P}}^o_{\mathcal{F}}|\mathcal{H}_0$ and the maximum of each $\underline{\mathbb{P}}^o_{\mathcal{F}}|\mathcal{H}_{i\neq 0}(\mathrm{b}_i)$.

Finally, to compute the maximum $\underline{\mathbb{P}}_{\mathcal{F}}(\mathbf{b})$, assumptions are needed for the a-priori $\mathsf{P}(\mathcal{H}_i)'s$ for $i \in \{0, ..., 15\}$. Since the alternative hypotheses account for outliers in the pseudoranges at the rover-receiver (automated vehicle), it is assumed that they primarily occur due to different signal reflections caused by the surrounding environment (e.g., nearby infrastructure). For this analysis we make three sets of assumptions ranging from conservative to optimistic cases: (i) $\mathsf{P}(\mathcal{H}_0) = 0.98500$ and $\mathsf{P}(\mathcal{H}_i) = 10^{-3}$ for $i \in \{1, ..., 15\}$, (ii) $\mathsf{P}(\mathcal{H}_0) = 0.99850$ and $\mathsf{P}(\mathcal{H}_i) = 10^{-4}$ for $i \in \{1, ..., 15\}$, (iii) $\mathsf{P}(\mathcal{H}_0) = 0.99985$ and $\mathsf{P}(\mathcal{H}_i) = 10^{-5}$ for $i \in \{1, ..., 15\}$. The obtained results for the maximum $\underline{\mathbb{P}}_{\mathcal{F}}(\mathbf{b})$ (see 23) in the three cases are shown in Table 4. The results from this subsection correspond to the receiver-satellite geometry shown in Figure 8(a) and to the *fixed* safety-region $\mathcal{B}$ depicted in Figure 8(b). However, in practice, the vehicle's orientation will change. Therefore, in the next section, we determine the maximum $\underline{\mathbb{P}}_{\mathcal{F}}(\mathbf{b})$ at the *worst orientation* of the vehicle with respect to the satellite geometry from Figure 8(a).

Table 4: Maximum values of $\underline{\mathbb{P}}_{\mathcal{F}}(\mathbf{b})$ and their standard deviations (σ_{sim}).

Cases	$\mathsf{P}(\mathcal{H}_0)$	Max. $\underline{\mathbb{P}}_{\mathcal{F}}(\mathbf{b})$	σ_{sim}
1	0.98500	$2.14 \cdot 10^{-7}$	$5.20 \cdot 10^{-9}$
2	0.99850	$2.15 \cdot 10^{-8}$	$5.20 \cdot 10^{-10}$
3	0.99985	$2.23 \cdot 10^{-9}$	$5.20 \cdot 10^{-11}$

c) Probability of positioning failure for different orientations of the safety-region $\mathcal{B}_\theta \subset \mathbb{R}^2$

A vehicle will change its orientation while moving (e.g., when making a U-turn, exiting a highway, taking a left/right turn). For a short time window (e.g., few minutes), it can be assumed that the receiver-satellite geometry from Figure 8(a) is constant, allowing us to base our next analysis on the vehicle's change in orientation. We re-express the safety-region from (37) to account for the dependence on the orientation angle θ, measured clockwise w.r.t. the vertical axis,

$$\mathcal{B}_\theta = \{h \in \mathbb{R}^2 \mid ||h - \mathrm{h}_{\text{true}}||^2_{\mathrm{Q}_{\mathcal{B}_\theta}} \leq 1\}, \tag{39}$$

where $\mathrm{Q}^{-1}_{\mathcal{B}_\theta}$ now depends on θ and $\theta \in [0° \;\; 180°]$. Next, we compute the maximum $\underline{\mathbb{P}}_{\mathcal{F}}(\mathbf{b})$ as a function of θ from its components $\underline{\mathbb{P}}_{\mathcal{F}}|\mathcal{H}_0$ and $\max\limits_{\mathrm{b}_1,...,\mathrm{b}_k} \sum_{i=1}^{15} \underline{\mathbb{P}}_{\mathcal{F}}|\mathcal{H}_i(\mathrm{b}_i)$. Figure 13(a) shows the variations of $\underline{\mathbb{P}}_{\mathcal{F}}|\mathcal{H}_0$ as a function of θ. As θ approaches $10°$, $\mathcal{B}_\theta$ captures most of the probability density of $f_{\underline{\bar{\mathrm{h}}}}(h|\mathcal{H}_0)$ reaching a minimum value of $9.54 \cdot 10^{-12} \pm 8.41 \cdot 10^{-14}$ for $\theta = 10°$ (see Figure 9). Once $\theta > 10°$ the values of $\underline{\mathbb{P}}_{\mathcal{F}}|\mathcal{H}_0$ starts to increase as some of the components of $f_{\underline{\bar{\mathrm{h}}}}(h|\mathcal{H}_0)$ will have a larger density outside $\mathcal{B}_\theta$ (see Figure 9), the maximum being reached at a value of $3.13 \cdot 10^{-7} \pm 2.11 \cdot 10^{-9}$ for $\theta = 110°$. A similar reasoning can be applied to the behaviour of $\max\limits_{\mathrm{b}_1,...,\mathrm{b}_k} \sum_{i=1}^{15} \underline{\mathbb{P}}_{\mathcal{F}}|\mathcal{H}_i(\mathrm{b}_i)$ in Figure 13(b).

By combining the results from Figures 13(a) and 13(b) with the assumptions regarding the a-priori probabilities $\mathsf{P}(\mathcal{H}_0)$ and $\mathsf{P}(\mathcal{H}_i)$ for $i \neq 0$, as discussed in the three cases presented in the previous section, the results in Figure 13(c) are obtained. In the most conservative case (Case 1), the maximum $\underline{\mathbb{P}}_{\mathcal{F}}(\mathbf{b})$ at $\theta = 110°$ is $1.84 \cdot 10^{-5} \pm 2.16 \cdot 10^{-9}$ while for the most optimistic (Case 3) is $4.94 \cdot 10^{-7} \pm 2.16 \cdot 10^{-9}$. Given that we are in a snapshot positioning scenario of an automated vehicle at decimeter-level with a horizontal positioning precision of about 0.5 meters (95% circular probability radius), while accounting for one-dimensional outliers in the observables, the result in Case 1 is rather high.

Table 5: Maximum values of $\underline{\mathbb{P}}_{\mathcal{F}}(\mathbf{b})$ at the worst-orientation of the vehicle w.r.t. the satellite geometry from Figure 8(a).

Cases	$\mathsf{P}(\mathcal{H}_0)$	Max. $\underline{\mathbb{P}}_{\mathcal{F}}(\mathbf{b})$ at $\theta = 110°$	σ_{sim}
1	0.98500	$1.84 \cdot 10^{-5}$	$2.16 \cdot 10^{-9}$
2	0.99850	$2.12 \cdot 10^{-6}$	$5.07 \cdot 10^{-9}$
3	0.99985	$4.94 \cdot 10^{-7}$	$2.16 \cdot 10^{-9}$

These results help determine whether the target requirements or guidelines for positioning safety are met at a particular time instant. This assessment is based on the assumed functional and stochastic models in (33), the receiver-satellite geometry in Figure 8(b), the safety-region $\mathcal{B}_\theta$ defined in (39), and the statistical hypothesis testing procedure in (34). If the requirements or

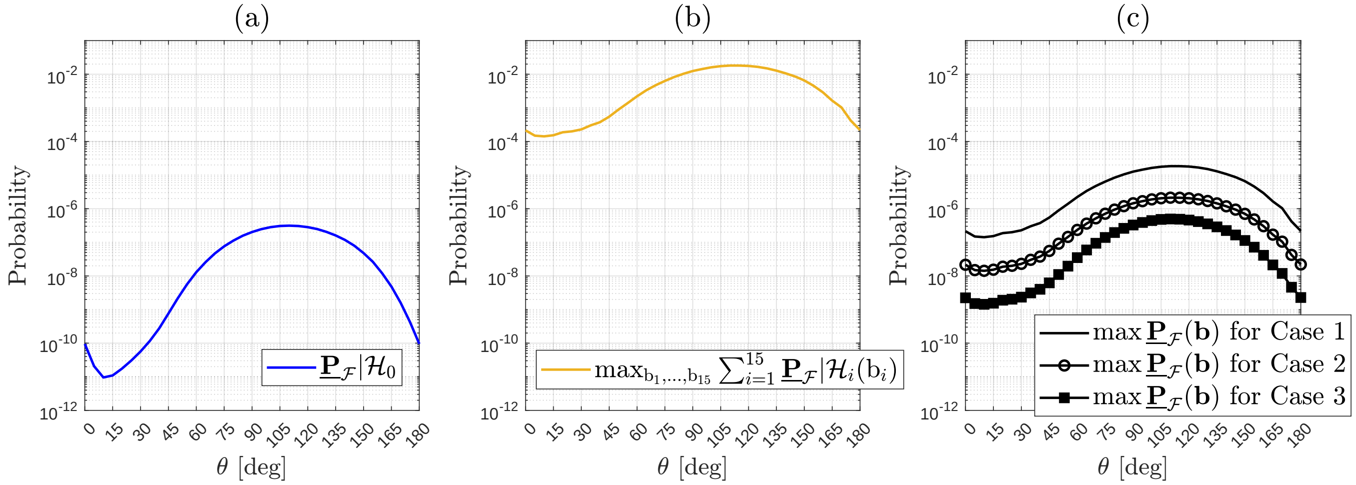

Figure 13: (a) Computed $\underline{\mathbb{P}}_{\mathcal{F}}|\mathcal{H}_0$ over the angles θ; (b) Computed $\max\limits_{\mathrm{b}_1,\ldots,\mathrm{b}_k} \sum_{i=1}^{k} \mathbb{P}_{\mathcal{F}}|\mathcal{H}_i(\mathrm{b}_i)$ over the angles θ; (c) Computed maximum total probability of positioning failure $\underline{\mathbb{P}}_{\mathcal{F}}(\mathbf{b})$ over the angles θ for the three cases: (i) Case 1 when the a-priori $\mathsf{P}(\mathcal{H}_0) = 0.98500$ and $\mathsf{P}(\mathcal{H}_i) = 10^{-3}$ for $i \in \{1, \ldots, 15\}$, (ii) Case 2 when the a-priori $\mathsf{P}(\mathcal{H}_0) = 0.99850$ and $\mathsf{P}(\mathcal{H}_i) = 10^{-4}$ for $i \in \{1, \ldots, 15\}$, and (iii) Case 3 when the a-priori $\mathsf{P}(\mathcal{H}_0) = 0.99985$ and $\mathsf{P}(\mathcal{H}_i) = 10^{-5}$ for $i \in \{1, \ldots, 15\}$.

guidelines are not satisfied, then appropriate changes in any of these elements, such as those related to the measurement setup (functional and stochastic models), safety-region, or the combined parameter estimation and statistical hypothesis testing procedure, may be necessary. For instance, the new theoretical framework introduced in (Teunissen, 2024a) shows how fit-for-purpose statistical hypothesis testing improves the performance of DIA-estimators.

V. SUMMARY AND FUTURE WORK

In this contribution we have presented an approach for positioning safety-analyses studies that can be carried out at the design stage, when choices are to be made regarding (i) measurement models, (ii) parameter estimation algorithms, (iii) statistical hypothesis testing procedures for model misspecifications (e.g., outliers in measurements), and (iv) positioning scenarios for vehicles, among others. At the design stage numerical simulations are needed to be able to deal with the complexity of the involved multiple integrals and also with the impracticability of collecting necessary data by having to drive millions or even billions of kilometers, as it would be the case for automated and autonomous driving (Kalra and Paddock, 2016)). Such an approach is in line with the scenario-based safety assessment framework used in studies for automated and autonomous vehicles (Riedmaier et al., 2020; U.N.E.C.E., 2023; de Gelder et al., 2024). Once compliance with the application-specific requirements is demonstrated on the basis of the probability of positioning failure in the scenarios of interest, the resulting parameter estimation and statistical hypothesis testing procedure can be implemented for real-time positioning.

We have accounted for the dependence between parameter estimation and statistical hypothesis testing via the DIA-estimator $\underline{\bar{x}} \in \mathbb{R}^n$ and its PDF $f_{\underline{\bar{x}}}(x)$ as introduced in (Teunissen, 2018). In this context, the event of the positioning failure $\mathcal{F} = \{\underline{\bar{x}} \in \mathcal{B}^c\}$ (page 15 in (RTCA-Special Committee 159, 2020)) and its probability $\underline{\mathbb{P}}_{\mathcal{F}}(\mathbf{b})$ are studied for a positioning scenario, at the decimetre-level, of an automated vehicle at a time instant (snapshot). On the basis of (i) a dual-constellation (GPS and Galileo) DGNSS positioning model, (ii) a horizontal positioning precision of about 0.5 meters (95% circular probability radius), (iii) a Detection, Identification, and Adaptation procedure for individual outliers in the observables, and (iv) an ellipticaly-shaped safety-region $\mathcal{B} \subset \mathbb{R}^2$ that inscribes the vehicle whose length is 4.5 [m] and width 1.8 [m], we have quantified the probability of positioning failure and its conditional components. Additionally, we have quantified these probabilities as a function of the vehicle's orientation w.r.t. the GNSS satellite geometry showing that the maximum $\underline{\mathbb{P}}_{\mathcal{F}}(\mathbf{b})$ varies across 2 orders of magnitude (Figure 13). It was also shown that for a conservative assumption on the a-priori probabilities of the occurrence of the hypotheses (Case 1), the maximum $\underline{\mathbb{P}}_{\mathcal{F}}(\mathbf{b})$ at the worst orientation of the vehicle ($\theta = 110°$ measured clockwise w.r.t. the vertical axis) is $1.84 \cdot 10^{-5} \pm 2.16 \cdot 10^{-9}$ (Table 5), which can be regarded as a high value when safety requirements or guidelines would demand it to be 10^{-7} or lower (at a particular time instant). While our positioning scenario was focused on the automotive domain, the approach to positioning safety analysis is also applicable to other safety-critical applications, such as aviation, shipping, and rail.

A topic for future work is the quantification of the probability of positioning-failure over a time-horizon $\Delta\tau$ (e.g., seconds, minutes, hours) within a scenario-based safety-assessment framework and using numerical simulation. The objective is to capture time-dependent effects, such as: (i) time-correlated measurement noise, (ii) time-dependent model misspecifications, (iii) variation of the satellite geometry, etc. The probability of positioning failure over a time horizon $\Delta\tau$ that also accounts for time-dependent failure-region $\mathcal{B}^c_{\theta_\tau} \subset \mathbb{R}^n$ and time-dependent PDF $f_{\underline{\mathrm{x}}}(x, \tau)$ can be expressed as,

$$\mathbb{P}_{\mathcal{F}}(\mathbf{b}_{\Delta\tau}, \Delta\tau) = \int_{\Delta\tau} \int_{\mathbb{R}^n} f_{\underline{\mathrm{x}}}(x, \tau)\, \mathbb{1}_{\mathcal{B}^c_{\theta_\tau}}(x, \tau)\, dx\, d\tau. \tag{40}$$

where the elements of $\mathbf{b}_{\Delta\tau}$ are accounted for in $f_{\underline{\mathrm{x}}}(x, \tau)$.

ACKNOWLEDGEMENTS

This research was funded by the Dutch Research Council (NWO) under Grant 18305 ”I-GNSS Positioning for Assisted and Automated Driving”. The authors acknowledge the use of computational resources of the DelftBlue supercomputer, provided by Delft High Performance Computing Centre (https://www.tudelft.nl/dhpc). All the support is gratefully appreciated.

REFERENCES

Baarda, W. (1967). Statistical Concepts in Geodesy. *Netherlands Geodetic Commission, Publications on Geodesy*, 2(4):1–74. `https://ncgeo.nl/index.php/en/publicatiesgb/publications-on-geodesy/item/2514-pog-08-w-baarda-statistical-concepts-in-geodesy`.

Baarda, W. (1968). A Testing Procedure for Use in Geodetic Networks. *Netherlands Geodetic Commission, Publ. Geod.*, 2(5):1–97. `https://www.ncgeo.nl/index.php/en/publicatiesgb/publications-on-geodesy/item/2515-pog-09-w-baarda-a-testing-procedure-for-use-in-geodetic-networks`.

Bancroft, T. A. (1944). On Biases in Estimation Due to the Use of Preliminary Tests of Significance. *Annals of Mathematical Statistics*, 15(2):190–204. `https://www.jstor.org/stable/2236199`.

Blanch, J. et al. (2015). Baseline Advanced RAIM User Algorithm and Possible Improvements. *IEEE Aerospace and Electronic Systems*, 51(1):713–732. `https://ieeexplore.ieee.org/document/7073524`.

Danilov, D. and Magnus, J. R. (2004). On the harm that ignoring pretesting can cause. *Journal of Econometrics*, 122(1):27–46. `https://www.sciencedirect.com/science/article/pii/S0304407603002689`.

de Gelder, E. et al. (2024). TNO Street Wise: Scenario-Based Safety Assessment of Automated Driving Systems. White paper, Netherlands Organisation for Applied Scientific Research (TNO). `https://www.tno.nl/en/newsroom/papers/scenario-based-safety-assessment/`.

Euler, H. J. and Goad, C. C. (1991). On optimal filtering of GPS dual frequency observations without using orbit information. *Bulletin Géodésique*, 65(2):130–143. `https://link.springer.com/article/10.1007/BF00806368`.

Feng, Y., Wang, C., and Karl, C. (2018). Determination of Required Positioning Integrity Parameters for Design of Vehicle Safety Applications. In *Proceedings of the ION GNSS+ Conference*, pages 129–141. `https://www.ion.org/publications/abstract.cfm?articleID=15556`.

Gillissen, I. and Elema, I. A. (1996). Test Results of DIA: A Real-Time Adaptive Integrity Monitoring Procedure, Used in an Integrated Navigation System. *International Hydrographic Review*, 73(1):75–103. `https://journals.lib.unb.ca/index.php/ihr/article/view/23166`.

Hauschild, A. (2017). Combination of Observations. In Teunissen, P. J. G. and Montenbruck, O., editors, *Handbook of Global Navigation Satellite Systems*, pages 594–596. Springer. `https://link.springer.com/book/10.1007/978-3-319-42928-1`.

Hwang, P. T. and Brown, R. G. (2006). RAIM-FDE Revisited: A New Breakthrough in Availability Performance With nioRAIM (Novel Integrity-Optimized RAIM). *NAVIGATION*, 53(1):41–51. `https://www.ion.org/publications/abstract.cfm?articleID=102414`.

Kalra, N. and Paddock, S. M. (2016). Driving to safety: How many miles of driving would it take to demonstrate autonomous vehicle reliability? *Transportation Research Part A*, 94:182–193. `https://www.sciencedirect.com/science/article/pii/S0965856416302129`.

Kealy, A. and Moore, T. (2017). Land-based Applications of GNSS (Chapter 29.1). In Teunissen, P. J. G. and Montenbruck, O., editors, *Springer Handbook of Global Navigation Satellite Systems*, pages 842–856. Springer. `https://link.springer.com/book/10.1007/978-3-319-42928-1`.

Kigotho, O. N. and Rife, J. H. (2021). Comparison of Rectangular and Elliptical Alert Limits for Lane-Keeping Applications. In *Proceedings of the ION GNSS+ Conference*, pages 93–104. `https://www.ion.org/publications/abstract.cfm?articleID=17904`.

Morton, Y. T. J., van Diggelen, F., Spilker, Jr., J. J., Parkinson, B. W., Lo, S., and Gao, G., editors (2020). *Position, Navigation, and Timing Technologies in the 21st Century: Integrated Satellite Navigation, Sensor Systems, and Civil Applications* . Wiley, IEEE Press. `https://onlinelibrary.wiley.com/doi/book/10.1002/9781119458449`.

Odijk, D. (2002). *Fast Precise GPS Positioning in the Presence of Ionospheric Delays* . PhD thesis, Delft University of Technology. `https://repository.tudelft.nl/record/uuid:40d49779-2ef4-4641-9ae4-f591871063fa`.

Odijk, D. (2017). Positioning Model (Chapter 21). In Teunissen, P. J. G. and Montenbruck, O., editors, *Springer Handbook of Global Navigation Satellite Systems*, pages 623–630. Springer. `https://link.springer.com/book/10.1007/978-3-319-42928-1`.

Reid, T. G. R. et al. (2019). Localization Requirements for Autonomous Vehicles. *SAE International Journal of Connected and Automated Vehicles*. `https://arxiv.org/abs/1906.01061`.

Riedmaier, S. et al. (2020). Survey on Scenario-Based Safety Assessment of Automated Vehicles. *IEEE Access*, 8:87456–87477. `https://ieeexplore.ieee.org/document/9090897`.

Robert, C. P. and Casella, G. (1999). *Monte Carlo Statistical Methods*. Springer. `https://link.springer.com/book/10.1007/978-1-4757-3071-5`.

Routtenberg, T. and Tong, L. (2016). Estimation After Parameter Selection: Performance Analysis and Estimation Methods. *IEEE Transactions on Signal Processing*, 64(20):5268–5281. `https://ieeexplore.ieee.org/document/7491362`.

RTCA-Special Committee 159 (2020). Minimum Operational Performance Standards (MOPS) for Global Positioning System/Satellite-Based Augmentation System Airborne Equipment. DO-229F, Radio Technical Commission for Aeronautics. `https://standards.globalspec.com/std/14281994/rtca-do-229`.

Teunissen, P. J. G. (1990). Nonlinear Least Squares. *Manuscripta Geodaetica*, 15(3):137–150. `https://espace.curtin.edu.au/handle/20.500.11937/38758`.

Teunissen, P. J. G. (2017). Batch and Recursive Model Validation (Chapter 24). In Teunissen, P. J. G. and Montenbruck, O., editors, *Springer Handbook of Global Navigation Satellite Systems*, pages 687–720. Springer. `https://link.springer.com/book/10.1007/978-3-319-42928-1`.

Teunissen, P. J. G. (2018). Distributional theory for the DIA method. *Journal of Geodesy*, 92(1):59–80. `https://link.springer.com/article/10.1007/s00190-017-1045-7`.

Teunissen, P. J. G. (2024a). On the optimality of DIA-estimators: theory and applications. *Journal of Geodesy*, 98(43):1–26. `https://link.springer.com/article/10.1007/s00190-024-01859-w`.

Teunissen, P. J. G. (2024b). *Testing Theory: An Introduction*. Mathematical Geodesy and Positioning Series. Delft University Press, 3rd edition. `https://pure.tudelft.nl/ws/portalfiles/portal/214132690/Testing_Theory.pdf`.

Teunissen, P. J. G. and Montenbruck, O., editors (2017). *Handbook of Global Navigation Satellite Systems*. Springer. `https://link.springer.com/book/10.1007/978-3-319-42928-1`.

U.N.E.C.E. (2023). New Assessment/Test Method for Automated Driving (NATM) Guidelines for Validating Automated Driving Systems (ADS). Report, United Nations Economic Commission for Europe - Inland Transport Committee). `https://unece.org/sites/default/files/2023-04/ECE-TRANS-WP.29-2023-44e.pdf`.

Yang, L., Li, Y., and Rizos, C. (2013). An enhanced MEMS-INS/GNSS integrated system with fault detection and exclusion capability for land vehicle navigation in urban areas. *GPS Solutions*, 18(4):593–603. `https://link.springer.com/article/10.1007/s10291-013-0357-1`.

Zaminpardaz, S. and Teunissen, P. J. G. (2022). On the computation of confidence regions and error ellipses: A critical appraisal. *Journal of Geodesy*, 96(10):1–18. `https://link.springer.com/article/10.1007/s00190-022-01596-y`.

Zaminpardaz, S. and Teunissen, P. J. G. (2023). Detection-only versus detection and identification of model misspecifications. *Journal of Geodesy*, 97(55):1–19. `https://link.springer.com/article/10.1007/s00190-023-01740-2`.

APPENDIX

V-A. Simulation procedure for the DIA-estimator

Parameter estimation and any statistical hypothesis testing procedure can be simulated by following the steps below:

1. Generate N i.i.d. pseudo-random samples of observations $\mathrm{y}^{(1)} \in \mathbb{R}^m, ..., \mathrm{y}^{(N)} \in \mathbb{R}^m$ from $f_{\underline{\mathrm{y}}}(y)$.
2. Compute the BLUEs under $\mathcal{H}_0$ and the misclosure vectors $\forall l \in \{1, ..., N\}$

$$\begin{bmatrix} \hat{\mathrm{x}}_0^{(l)} \\ \mathrm{t}^{(l)} \end{bmatrix} = \begin{bmatrix} (\mathrm{A}^T \mathrm{Q}_{\mathrm{yy}}^{-1} \mathrm{A})^{-1} \mathrm{A}^T \mathrm{Q}_{\mathrm{yy}}^{-1} \\ \mathrm{B}^T \end{bmatrix} \mathrm{y}^{(l)}. \tag{41}$$

3. Compute the indicator functions given the partitions $\mathcal{P}_i \subset \mathbb{R}^r$ for $\forall i \in \{0, ..., k\}$ and $\forall l \in \{1, ..., N\}$

$$p_i(\mathrm{t}^{(l)}) = \begin{cases} 1, & \text{if } \mathrm{t}^{(l)} \in \mathcal{P}_i \\ 0, & \text{otherwise} \end{cases}. \tag{42}$$

4. Formulate the DIA-estimate $\forall l \in \{1, ..., N\}$

$$\bar{\mathrm{x}}^{(l)} = \sum_{i=0}^{k} \hat{\mathrm{x}}_i^{(l)} p_i(\mathrm{t}^{(l)}) = \hat{\mathrm{x}}_0^{(l)} - \sum_{i=1}^{k} \mathrm{L}_i \, \mathrm{t}^{(l)} p_i(\mathrm{t}^{(l)}). \tag{43}$$

V-B. Correlation coefficient from Section IV.1 for a general structure of the variance-covariance matrix of the observables

The same models in (24) are kept, except Q_{yy}. We consider a more general structure

$$\mathrm{Q}_{\mathrm{yy}} = \begin{bmatrix} \sigma_{y_1}^2 & \rho \, \sigma_{y_1} \sigma_{y_2} \\ \rho \, \sigma_{y_1} \sigma_{y_2} & \sigma_{y_2}^2 \end{bmatrix}. \tag{44}$$

The correlation coefficient can be obtained for the cases below.

- Case 1: $\rho = 0, \; \sigma_{y_1}^2 = \sigma_{y_2}^2 \rightarrow \rho_{\underline{\hat{\mathrm{x}}}_1, \underline{\mathrm{t}}} = -\frac{\sqrt{2}}{2}$,
- Case 2: $\rho = 0, \; \sigma_{y_1}^2 \neq \sigma_{y_2}^2 \rightarrow \rho_{\underline{\hat{\mathrm{x}}}_1, \underline{\mathrm{t}}} = -\frac{\sigma_{y_2}}{\sqrt{\sigma_{y_1}^2 + \sigma_{y_2}^2}}$,
- Case 3: $\rho \neq 0, \; \sigma_{y_1}^2 = \sigma_{y_2}^2 \rightarrow \rho_{\underline{\hat{\mathrm{x}}}_1, \underline{\mathrm{t}}} = -\frac{\sqrt{2}}{2} \sqrt{(1 - \rho)}$,
- Case 4: $\rho \neq 0, \; \sigma_{y_1}^2 \neq \sigma_{y_2}^2 \rightarrow \rho_{\underline{\hat{\mathrm{x}}}_1, \underline{\mathrm{t}}} = -\frac{\sigma_{y_2}^2 - \rho \sigma_{y_1} \sigma_{y_2}}{\sqrt{\sigma_{y_1}^2 \sigma_{y_2}^2 (1 - \rho^2) + (\sigma_{y_2}^2 - \rho \sigma_{y_1} \sigma_{y_2})^2}}$.

V-C. Tables with maximum probabilities of positioning failure per hypotheses

The results in Table 6 (when the dependence between parameter estimation and statistical hypothesis testing is accounted for) show several cases for which there are significant differences w.r.t. the ones in Table 7 (when the dependence is *ignored*). Some examples are: (i) $\underline{\mathbb{P}}_{\mathcal{F}}^{o} | \mathcal{H}_0$ is 341 times lower than $\underline{\mathbb{P}}_{\mathcal{F}} | \mathcal{H}_0$, (ii) $\underline{\mathbb{P}}_{\mathcal{F}}^{o} | \mathcal{H}_1(\mathrm{b}_1)$ is ≈127 times lower than $\underline{\mathbb{P}}_{\mathcal{F}} | \mathcal{H}_1(\mathrm{b}_1)$, (iii) $\underline{\mathbb{P}}_{\mathcal{F}}^{o} | \mathcal{H}_5(\mathrm{b}_5)$ is ≈373 times lower than $\underline{\mathbb{P}}_{\mathcal{F}} | \mathcal{H}_5(\mathrm{b}_5)$, (iv) $\underline{\mathbb{P}}_{\mathcal{F}}^{o} | \mathcal{H}_9(\mathrm{b}_9)$ is ≈586 times lower than $\underline{\mathbb{P}}_{\mathcal{F}} | \mathcal{H}_9(\mathrm{b}_9)$, and (v) $\underline{\mathbb{P}}_{\mathcal{F}}^{o} | \mathcal{H}_{15}(\mathrm{b}_{15})$ is ≈203 times lower than $\underline{\mathbb{P}}_{\mathcal{F}} | \mathcal{H}_{15}(\mathrm{b}_{15})$. These differences indicate a significant deviation of $f_{\underline{\bar{\mathrm{h}}}}(h | \mathcal{H}_0)$ and of $f_{\underline{\bar{\mathrm{h}}}}(h | \mathcal{H}_j)$, for $j \in \{1, 5, 9, 15\}$, from Gaussian PDFs. Conversely, for $j \in \{4, 10, 12, 14\}$, we have that (i) $\underline{\mathbb{P}}_{\mathcal{F}}^{o} | \mathcal{H}_4(\mathrm{b}_4)$ is ≈6 times lower than $\underline{\mathbb{P}}_{\mathcal{F}} | \mathcal{H}_4(\mathrm{b}_4)$, (ii) $\underline{\mathbb{P}}_{\mathcal{F}}^{o} | \mathcal{H}_{10}(\mathrm{b}_{10})$ is ≈3 times lower than $\underline{\mathbb{P}}_{\mathcal{F}} | \mathcal{H}_{10}(\mathrm{b}_{10})$, (iii) $\underline{\mathbb{P}}_{\mathcal{F}}^{o} | \mathcal{H}_{12}(\mathrm{b}_{12})$ is ≈3 times lower than $\underline{\mathbb{P}}_{\mathcal{F}} | \mathcal{H}_{12}(\mathrm{b}_{12})$, and (iv) $\underline{\mathbb{P}}_{\mathcal{F}}^{o} | \mathcal{H}_{14}(\mathrm{b}_{14})$ is ≈2 times lower than $\underline{\mathbb{P}}_{\mathcal{F}} | \mathcal{H}_{14}(\mathrm{b}_{14})$. In these cases, the corresponding PDFs $f_{\underline{\bar{\mathrm{h}}}}(h | \mathcal{H}_j)$, for $j \in \{4, 10, 12, 14\}$ do not show a deviation as significant as the previous cases and hence the differences in the results being less severe.

Table 6: When the dependence is accounted for: Computed $\mathbb{P}_{\mathcal{F}}|\mathcal{H}_0$ and $\mathbb{P}_{\mathcal{F}}|\mathcal{H}_{i\neq 0}(\mathrm{b}_i)$, their maximum value, simulation standard deviation, and the magnitude of the model outlier where the maximum occurs

Component	Max. value	σ_{sim}	$\lvert\mathrm{b}_i\rvert$ [m]
$\mathbb{P}_{\mathcal{F}}\lvert\mathcal{H}_0$	$9.50 \cdot 10^{-11}$	$8.42 \cdot 10^{-13}$	-
$\mathbb{P}_{\mathcal{F}}\lvert\mathcal{H}_1(\mathrm{b}_1)$	$4.65 \cdot 10^{-7}$	$1.62 \cdot 10^{-8}$	2.66
$\mathbb{P}_{\mathcal{F}}\lvert\mathcal{H}_2(\mathrm{b}_2)$	$3.18 \cdot 10^{-9}$	$1.40 \cdot 10^{-10}$	1.73
$\mathbb{P}_{\mathcal{F}}\lvert\mathcal{H}_3(\mathrm{b}_3)$	$2.78 \cdot 10^{-6}$	$5.06 \cdot 10^{-8}$	1.79
$\mathbb{P}_{\mathcal{F}}\lvert\mathcal{H}_4(\mathrm{b}_4)$	$3.19 \cdot 10^{-5}$	$2.15 \cdot 10^{-6}$	2.17
$\mathbb{P}_{\mathcal{F}}\lvert\mathcal{H}_5(\mathrm{b}_5)$	$5.87 \cdot 10^{-9}$	$2.33 \cdot 10^{-10}$	1.39
$\mathbb{P}_{\mathcal{F}}\lvert\mathcal{H}_6(\mathrm{b}_6)$	$1.37 \cdot 10^{-9}$	$4.43 \cdot 10^{-11}$	3.82
$\mathbb{P}_{\mathcal{F}}\lvert\mathcal{H}_7(\mathrm{b}_7)$	$1.79 \cdot 10^{-7}$	$1.10 \cdot 10^{-8}$	3.06
$\mathbb{P}_{\mathcal{F}}\lvert\mathcal{H}_8(\mathrm{b}_8)$	$3.77 \cdot 10^{-5}$	$2.96 \cdot 10^{-6}$	3.12
$\mathbb{P}_{\mathcal{F}}\lvert\mathcal{H}_9(\mathrm{b}_9)$	$2.16 \cdot 10^{-9}$	$1.98 \cdot 10^{-11}$	4.12
$\mathbb{P}_{\mathcal{F}}\lvert\mathcal{H}_{10}(\mathrm{b}_{10})$	$4.35 \cdot 10^{-5}$	$2.86 \cdot 10^{-6}$	2.10
$\mathbb{P}_{\mathcal{F}}\lvert\mathcal{H}_{11}(\mathrm{b}_{11})$	$1.83 \cdot 10^{-6}$	$2.41 \cdot 10^{-7}$	1.66
$\mathbb{P}_{\mathcal{F}}\lvert\mathcal{H}_{12}(\mathrm{b}_{12})$	$3.67 \cdot 10^{-7}$	$8.58 \cdot 10^{-9}$	2.90
$\mathbb{P}_{\mathcal{F}}\lvert\mathcal{H}_{13}(\mathrm{b}_{13})$	$3.46 \cdot 10^{-9}$	$1.45 \cdot 10^{-10}$	4.91
$\mathbb{P}_{\mathcal{F}}\lvert\mathcal{H}_{14}(\mathrm{b}_{14})$	$9.83 \cdot 10^{-5}$	$2.72 \cdot 10^{-6}$	1.83
$\mathbb{P}_{\mathcal{F}}\lvert\mathcal{H}_{15}(\mathrm{b}_{15})$	$2.67 \cdot 10^{-8}$	$4.36 \cdot 10^{-9}$	1.45

Table 7: When the dependence is ignored: Computed $\mathbb{P}^o_{\mathcal{F}}|\mathcal{H}_0$ and $\mathbb{P}^o_{\mathcal{F}}|\mathcal{H}_{i\neq 0}(\mathrm{b}_i)$, their maximum value, simulation standard deviation, and the magnitude of the model outlier where the maximum occurs.

Component	Max. value	σ_{sim}	$\lvert\mathrm{b}_i\rvert$ [m]
$\mathbb{P}_{\mathcal{F}}\lvert\mathcal{H}^o_0$	$2.78 \cdot 10^{-13}$	$2.78 \cdot 10^{-15}$	-
$\mathbb{P}^o_{\mathcal{F}}\lvert\mathcal{H}_1(\mathrm{b}_1)$	$3.66 \cdot 10^{-9}$	$1.86 \cdot 10^{-10}$	3.15
$\mathbb{P}^o_{\mathcal{F}}\lvert\mathcal{H}_2(\mathrm{b}_2)$	$5.93 \cdot 10^{-11}$	$1.65 \cdot 10^{-12}$	2.05
$\mathbb{P}^o_{\mathcal{F}}\lvert\mathcal{H}_3(\mathrm{b}_3)$	$8.20 \cdot 10^{-8}$	$2.37 \cdot 10^{-9}$	2.13
$\mathbb{P}^o_{\mathcal{F}}\lvert\mathcal{H}_4(\mathrm{b}_4)$	$5.28 \cdot 10^{-6}$	$1.23 \cdot 10^{-7}$	2.51
$\mathbb{P}^o_{\mathcal{F}}\lvert\mathcal{H}_5(\mathrm{b}_5)$	$1.58 \cdot 10^{-11}$	$2.40 \cdot 10^{-13}$	1.39
$\mathbb{P}^o_{\mathcal{F}}\lvert\mathcal{H}_6(\mathrm{b}_6)$	$1.61 \cdot 10^{-11}$	$2.74 \cdot 10^{-13}$	3.82
$\mathbb{P}^o_{\mathcal{F}}\lvert\mathcal{H}_7(\mathrm{b}_7)$	$5.54 \cdot 10^{-9}$	$9.15 \cdot 10^{-11}$	3.63
$\mathbb{P}^o_{\mathcal{F}}\lvert\mathcal{H}_8(\mathrm{b}_8)$	$2.90 \cdot 10^{-6}$	$6.88 \cdot 10^{-8}$	3.12
$\mathbb{P}^o_{\mathcal{F}}\lvert\mathcal{H}_9(\mathrm{b}_9)$	$3.69 \cdot 10^{-12}$	$7.18 \cdot 10^{-14}$	4.12
$\mathbb{P}^o_{\mathcal{F}}\lvert\mathcal{H}_{10}(\mathrm{b}_{10})$	$1.28 \cdot 10^{-5}$	$2.70 \cdot 10^{-7}$	2.10
$\mathbb{P}^o_{\mathcal{F}}\lvert\mathcal{H}_{11}(\mathrm{b}_{11})$	$5.83 \cdot 10^{-8}$	$1.52 \cdot 10^{-9}$	1.66
$\mathbb{P}^o_{\mathcal{F}}\lvert\mathcal{H}_{12}(\mathrm{b}_{12})$	$1.18 \cdot 10^{-7}$	$8.29 \cdot 10^{-10}$	2.90
$\mathbb{P}^o_{\mathcal{F}}\lvert\mathcal{H}_{13}(\mathrm{b}_{13})$	$6.79 \cdot 10^{-11}$	$2.45 \cdot 10^{-12}$	4.91
$\mathbb{P}^o_{\mathcal{F}}\lvert\mathcal{H}_{14}(\mathrm{b}_{14})$	$5.08 \cdot 10^{-5}$	$2.39 \cdot 10^{-7}$	1.83
$\mathbb{P}^o_{\mathcal{F}}\lvert\mathcal{H}_{15}(\mathrm{b}_{15})$	$1.31 \cdot 10^{-10}$	$9.41 \cdot 10^{-12}$	1.99